Electronic Supporting Information

Blue-Emitting InP Quantum Dots Participate in an Efficient Resonance Energy Transfer Process in Water

Pradyut Roy, Mishika Virmani, and Pramod P. Pillai*

Email: pramod.pillai@iiserpune.ac.in

Department of Chemistry, Indian Institute of Science Education and Research (IISER) Pune, Dr. Homi Bhabha Road, Pashan, Pune – 411 008, India.

Section 1: Experimental Details and Methods

Materials and Methods: Indium iodide (InI_3), zinc iodide (ZnI_2), zinc stearate ($Zn(St)_2$) olylamine (OAm), 1-octadecene (ODE), 1-dodecanethiol (DDT), 11-mercaptoundecanoic acid (MUA) and rhodamine B were purchased from Sigma-Aldrich and were used without further purification.

Synthesis of Pure-Blue Emitting InP/ZnS Quantum Dots:

The synthesis of pure-blue emitting InP/ZnS QDs was carried out by following a modified one-pot synthetic procedure.[1] In a typical synthesis, indium (III) iodide (0.34 mmol, 169 mg), zinc iodide (2.2 mmol, 703 mg) and olylamine (15 mmol, 5.0 mL) were taken in 100 mL three neck RB and heated to ~140 ^{0}C under Ar atmosphere with gentle stirring, till a clear solution was formed. The reaction mixture was degassed for ~60 min at 140 ^{0}C and the temperature was raised further to ~200 ^{0}C under inert atmosphere. Upon reaching 200 ^{0}C, 450 µL of tris-(dimethylamino) phosphine (2.47 mmol) in 1.0 mL of olylamine was quickly injected into the reaction mixture and kept for ~20 min for the growth of InP core QDs. An in-situ ZnS shell coating was performed to stabilize the QDs and improve the PL QY.

After 20 min, a solution of zinc and sulphur precursor was quickly injected into the reaction mixture at ~200 ^{0}C, which contained 6.6 mmol of DDT (~645 µL) and 1.0 mmol of zinc stearate in 4 mL ODE. Then the reaction temperature was raised to ~300 ^{0}C and allowed to react for ~45 min. At the end, the reaction mixture was quenched with water bath followed by addition of 5.0 mL hexane to arrest the growth of ZnS Shell. The obtained QD solution was centrifuged at 7000 rpm for 10 min to remove excess indium and zinc precursor. The resultant supernatant was purified by precipitating with ethanol and redispersed back in chloroform, and used for the further studies. The combination of DDT and zinc stearate was crucial in getting fine-control over the thickness of ZnS shell.

Dispersion of Pure-Blue Emitting InP/ZnS Quantum Dots in Water:

Water dispersed pure-blue emitting InP/ZnS QDs were prepared via the ligand exchange with MUA ligand.[2] In a typical place exchange protocol, MUA (~100 mg, 0.46 mmol) was dissolved in 1:4 ratio of water/methanol mixture (300 µL and 1.2 mL, respectively) and the pH of the solution was adjusted to ~12 using 3N NaOH solution. To the above solution of negatively charged MUA ligands, ~144 mmol of QD solution (~800 µL, 180 M) in chloroform was added, and stirred vigorously for ~5 min. Then, the solution was stirred for overnight followed by

addition of 2 mL of water and 6 mL of chloroform, to facilitate the complete transfer of QDs from organic to aqueous phase. The success of place exchange reaction can be easily monitored by observing the phase transfer of blue luminescence from chloroform (luminescence to non-luminescence) to water (non-luminescence to luminescence) layers. Then the aqueous phase was carefully separated and precipitated with acetone, to remove the unreacted MUA ligands via centrifugation. Finally, the anionic [-] InP/ZnS were redispersed in milli-Q water for further studies.

Instrumentation and Software

UV-vis Absorption Studies: UV-vis absorption studies were carried out on a Shimadzu UV-2600 UV/Vis spectrophotometer in an optical quartz cuvette of 1 cm path length over the range of 200-700 nm.

Steady-State Photoluminescence Studies: The photoluminescence experiments were performed on Fluoromax-4 spectrofluorometer (Horiba Jobin Yvon) with Xe-lamp as excitation source. The wavelength of excitation was 370 nm for donor InP/ZnS QD and [-] InP/ZnS QD:::Rh B complex, respectively.

Absolute Photoluminescence Quantum Yield Measurements (PL QY_A): The absolute PL quantum yield (PL QY_A) measurement was carried out by using an integrating sphere on Fluoromax-4 spectrofluorometer (Horiba Jobin Yvon) with Xe-lamp as excitation source. The wavelength of excitation was 350 nm, and the emission monochromator was set in between 340-690 nm for measuring the scattering for solvent and QY for sample.

Excitation Spectra: The excitation spectra were recorded using a Fluoromax-4 spectrofluorometer (Horiba Scientific) with Xe lamp as excitation source. The excitation monochromator was set between 300-450 nm for InP/ZnS donor QD, and 300-565 nm for acceptor Rh B dye. The emission monochromator was set at the PL maxima of the corresponding QDs and dye, to collect the excitation spectra of donor and acceptor materials.

Time-Corelated Single Photon Count (TCSPC) Measurements: Time-resolved studies were performed in a HORIBA DeltaFlex Time-Correlated Single Photon Counting system using 370 nm Delta-diode as the excitation source with a time to amplitude converter (TAC) range of 3.2 μs for 10,000 counts. The decay curve was deconvoluted using EZ analysis software and data was fit with four exponential curves. The average lifetime was calculated using the following equation.

$$\boldsymbol{\tau_{Avg}} = \frac{\sum_{i=1}^{i=4} \boldsymbol{\alpha_i \tau_i^2}}{\sum_{i=1}^{i=4} \boldsymbol{\alpha_i \tau_i}} \quad \textbf{... (1)}$$

Where τ_i is the lifetime and α_i is the pre-exponential factor.

The fractional contribution of each decay time (f_i) in the fit was calculated using the following equation.

$$\boldsymbol{f_i} = \frac{\boldsymbol{\alpha_i \tau_i}}{\sum \boldsymbol{\alpha_i \tau_i}}$$

Zeta Potential Measurements: The zeta potential (ζ) measurement of [-] InP/ZnS QDs was performed in Zetasizer Nano series, Nano-2590 (Malvern instruments, U.K.) with a 655 nm laser. The optical density of the solution was maintained ~0.03 during all the measurements. The ζ value was estimated from the electrophoretic mobility (U_E) (the velocity with which the charged particles are attracted to the oppositely charged electrodes) and is calculated using Henry's equation:

$$\boldsymbol{U_E} = \frac{\boldsymbol{2\varepsilon\zeta f(K_a)}}{\boldsymbol{3\eta}} \quad \textbf{... (2)}$$

Where,

ε is the dielectric constant.

ζ is the zeta potential (mV).

η is the viscosity coefficient of the medium (Pa.s).

f(ka) is Henry's function determined using Smoluchowski's approximation.

X-Ray Diffraction (XRD) Measurements: X-Ray diffraction patterns were measured on Bruker D8 Advanced X-Ray Diffractometer using Cu K_α (λ = 1.54 Å) rays. The samples for XRD analysis were prepared by drop casting the as synthesized QDs on a clean glass substrate.

High Resolution Transmission Electron Microscopy (HRTEM): The samples for microscopy measurements were prepared by drop casting QD solution on a 400-mesh carbon coated copper TEM grid (Ted Pella, Inc.). The samples were allowed to dry under ambient conditions, and were further dried under vacuum. The high-resolution images were recorded on a TALOS F200S G2 (200 keV) HRTEM instrument.

Fourier-Transform Infrared Spectroscopy (FTIR) Studies: Fourier transform infrared spectroscopy (FTIR) experiments were performed to confirm the presence of ligands on the surface of QDs. The measurements were performed on NICOLET 6700 FTIR instrument, using solid KBr disc.

X-ray Photoelectron Spectroscopy (XPS) Studies: The XPS study was performed by drop casting the QDs on silicon wafer, dispersed in IPA solvent, followed by drying under the vacuum. Then the measurements were performed in Thermo Fisher Scientific Instrument, Leicestershire, UK (Model: K-Alpha+) equipment using Al-Kα anode (1486.6 eV) in a transmission lens mode and multi-channel plate (MCP) detector. The binding energy scale was calibrated using standard C 1s peak (284.6 eV) and the elemental peaks were analysed using non-linear Shirley background correction. The peak positions fitting was performed by using Fityk software and optimized by a weight least-square fitting method using Gaussian and Lorentzian lineshape.

Nuclear Magnetic Resonance Spectroscopy (NMR) Studies: The ^{1}H NMR data was recorded on Brucker Ascend ^{TM} 400 MHz spectrometer.

Inductively Coupled Plasma-Mass Spectrometry (ICP-MS): The ICP-MS analysis was performed to determine the concentration of In^{3+} ion in InP/ZnS QD. At first, the QD sample was digested in 0.3 N HNO_3 solution, followed by filtration through syringe filter to remove any dust particles present in the solution. The amount of In^{3+} in the digested samples was quantified using ICP-MS analysis, performed on Quadrupole-ICP MS (Thermo iCAP-Q) instrument.

Cyclic Voltammetry (CV) Experiments: The CV measurements were performed using Metrohm DropSens μStat400 electrochemical workstation and Dropview 8400 software of version 2.215B1204. Glassy carbon was used as the working electrode, $Ag/AgNO_3$ as the reference electrode and Pt wire was used as the counter electrode.

Cytotoxicity and Bio-Imaging Studies: The MTT assay was measured using a Varioscan^{TM} plate reader instrument. For bio-imaging study, Zeiss LSM 780 confocal microscopy was used. Alongside, for maintaining the cells in tissue culture, we routinely use the following instruments: CO_2 incubator (galaxy 170, Eppendorf), centrifuge machines (5910 Ri, Eppendorf).

Cell Viability Assay: MTT assay was employed to understand cellular viability in response to the QDs.[3] Briefly, a 96 well glass bottom plate was seeded with Hela cells at a density of 1000 cells per well. The cells were allowed to grow and adjust to the artificially created atmosphere in a humidified environment balanced with 5% CO_2 and maintained at 37 ^oC. After 24 hours, the wells were aspirated off the media and replenished with QDs containing fresh media at various concentrations. Twelve concentrations were triplicated per QD and, were added for a given 96 well experiment. The first row of 6 well plate was kept as a control wherein no compound addition was made. The cells incubated with the compounds were left undisturbed under standard culture conditions for a period of 72 h. Towards the end of 72 h, the media in the plates were aspirated and a 50 µg/mL solution of MTT (3-(4,5-Dimethylthiazol-2-yl)-2,5-Diphenyltetrazolium Bromide) in complete media was added per well for a period of 4 h. After 4 h, the plates were carefully aspirated off the media without disturbing the settled formazan crystals and 100 µL of HPLC grade DMSO was then added to each well. The plate was then transferred to a microplate shaker and allowed the crystals to dissolve in DMSO for a total of 30 minutes. Next, the plate was then subjected under a Varioscan machine wherein the absorbance per well was then measured at 570 nm. The absorbance readout was then converted into the relative cellular viability with respect to the control, and was then plotted against the concentration.

Concentration Dependent Cellular Imaging: The six well sterile mammalian culture plate was employed for cellular uptake experiment of the quantum dots. A thoroughly cleaned and UV sterile coverslip was placed per well of a 6 well plate. Next the plate was left under the conditions of UV for a period of 30 minutes inside the laminar flow hood. A total of 105 cells dispersed in 2 mL of complete media were added per well on top of coverslip. The cells were then allowed to grow for a period of 16–24 h. Once the cells adhered with a visible and healthy cytoskeleton, the compound addition was attempted. For concentration optimization, cells were treated with different concentrations of QDs (20 µg/mL, 40 µg/mL) for a period of 6 h. At the end of 6 h, the media containing the compound was aspirated and washed 3 times with 2 mL warm HBBS buffer (Hank's balanced salt solution) to wash off the uninternalized QDs. Next, the cells were added with 1 mL of 4 % paraformaldehyde (PFA) solution and left undisturbed at room temperature for a period of 10 minutes. After 10 minutes, the cells were washed off with 2 mL warm HBBS solution twice to remove the PFA. The coverslip containing the fixed cells were then inverted onto a glass slide containing a drop (40 µL) of mounting media (70 %

glycerol in water). The seals of the glass slides to cover slips were carefully sealed using a transparent nail paint. The slides were then imaged under a confocal microscope.

Lysotracker Colocalization Experiment: To understand the position of QDs inside the cells, a colocalization experiment was performed with a commercially available lysotracker red dye (Lysotracker^{TM} Red DND- 99). A six well plate with a coverslip was added with 105 cells and then allowed to adhere. Next, the media was replenished with fresh media containing 40 µg/mL of QD system. After 6 h, the media was aspirated, and cells were washed thrice with 2 mL of HBBS buffer. Next a 0.1 µg/mL of Lysotracker red was added for additional 1 h. The cells were again washed with HBBS, fixed, and inverted onto a glass slide for confocal imaging.

Multicolor Imaging: Multicolor imaging experiments were performed under the experimental condition similar to the Lysotracker Colocalization study with QD concentration of 40 µg/mL. After initial treatments with QD solutions, the cells were incubated with SYTO^{TM} Deep Red at a concentration of 0.1 µg/mL in complete media for a total of 30-40 minutes. The cells were then washed twice with warm HBBS solution and fixed using paraformaldehyde fixation as described previously. Next, 100 µL of phalloidin (PHD) solution at 10^{-8} M concentration was then added onto the cover slip and was allowed to incubate under toom temperature conditions in dark for 2 h. Next, the cover slips containing cells were then rinsed off with warm HBBS solution and inverted onto a glass slide using 70 % glycerol in water as mounting media. The prepared glass slides were then imaged under a confocal microscope using 405 nm (Laser Power: 2%, Gain: 600) excitation laser for QD and collection from 415-500 nm range. The FITC conjugated phalloidin was excited using a 488 nm laser (Laser Power: 6%, Gain: 700) and the emission was collected in 510-560 nm range. The nuclear staining SYTO dye was excited using a 633 nm (Laser Power: 4%, Gain: 700). Stacks of dept 0.3 µm were collected per channel. The multicolour scanning was done on Zeiss Confocal instrument. The images collected were then processed using an ImageJ software for image processing and quantification.

Energy Transfer Experiments: The energy transfer experiments were performed with negatively charged [-] InP/ZnS QD and Rh B dye in water. In a typical energy transfer experiment, a 2.7 mL aqueous solution of donor InP/ZnS QDs was prepared with an absorbance was ~0.1 at the first excitonic peak (~410 nm), corresponding to ~4 µM of QD concentration. Next, different aliquots of acceptor Rh B dye (3 µL of ~700 µM) were sequentially added to donor InP/ZnS QD, and the PL spectral changes were monitored using Fluoromax-4

spectrofluorometer (HORIBA Scientific) under 370 nm excitation. The corresponding lifetime experiments were carried out in a HORIBA DeltaFlex Time-Correlated Single Photon Counting system using a 370 nm Delta-Diode source. The fluorescence decay was deconvoluted using EZ software, and fit with exponential decay, minimizing the χ^2 values.

Droplet Experiments: In a typical experiment, a glass slide was wrapped with a Teflon tape to increase the hydrophobicity of the substrate, so that uniform droplets can be prepared from aqueous samples. Following this, ~10 µL of (i) different ratios of donor-acceptor solution, (ii) only donor, and (iii) only acceptor solution was placed over the Teflon coated glass slide and allowed them for normal evaporation. The true colour PL images were taken at different time intervals.

Preparation of Agarose Gel: In a typical procedure, ~30 mg of agarose powder was taken in 3 mL water (1.0 % w/v), and heated at ~90 ^{o}C to completely solubilize agarose. The clear solution was cooled to 50 ^{o}C and then mixed with aqueous solutions of. (i) different ratios of donor-acceptor, (ii) only donor, and (iii) only acceptor. Finally, the agarose mixture was poured into petri dish and kept overnight at ~50 ^{0}C for film casting. The film was thoroughly characterised using steady-state and time-resolved spectroscopic techniques.

Section 2: Characterization of Quantum Dots

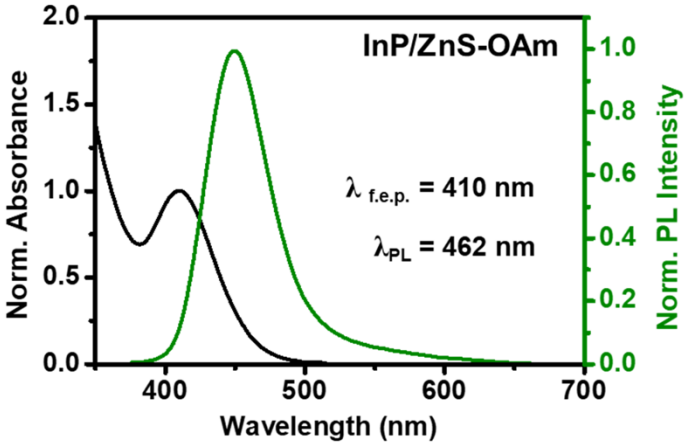

Fig. S1 The normalized UV-vis absorption and steady-state PL spectra of pure-blue emitting InP/ZnS QD in $CHCl_3$, capped with olylamine ligands. The wavelength of excitation was 370 nm.

Commission Internationale de l'Elcairage (CIE) Plot: The CIE plot was generated from GOCIE-1931 software.[4] The complete PL spectrum of pure-blue emitting InP/ZnS QD was used to generate the coordinate in CIE spectrum and, accordingly the colour purity was determined by calculating the deviation of the measured coordinate (for sample) from the

boundary of chromaticity diagram with respect to pure white region (0.33,0.33). Purity of colour, C_s, was determined by following the equation below.[4]

$$\boldsymbol{Color\ Purity} = \left(\frac{C_s - C}{C_b - C}\right) * \mathbf{100}\ \% \qquad \text{... (3)}$$

Where, C_s, C_b, and C represents the coordinates for sample, boundary, and centre of chromaticity diagram, respectively. The coordinates for boundary (C_b) were determined by connecting the sample point with the centre followed by extrapolating towards the boundary.

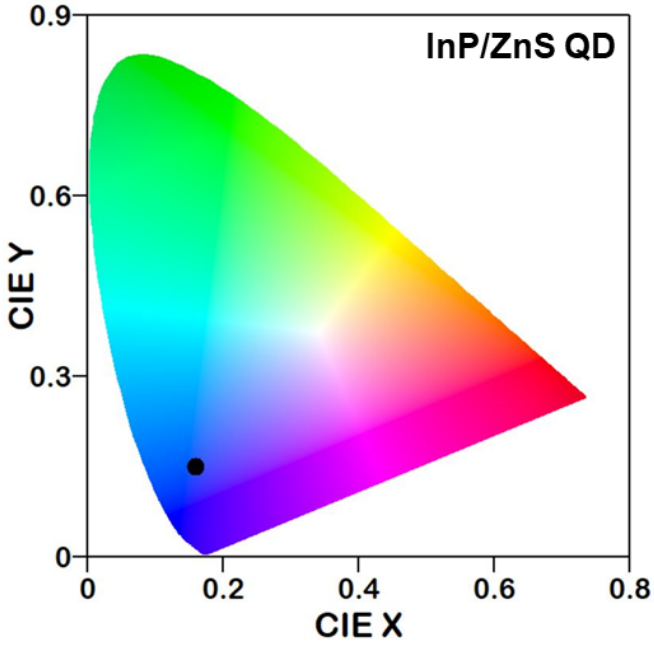

Fig. S2 The CIE 1931 plot for pure-blue emitting InP/ZnS QD. The corresponding fluorescence spectra to CIE axis point was estimated to be (0.16, 0.15). The measured colour purity was ~80 %.

Absolute PL QY Measurements of InP/ZnS QD Dispersed in Organic and Aqueous Solvents:

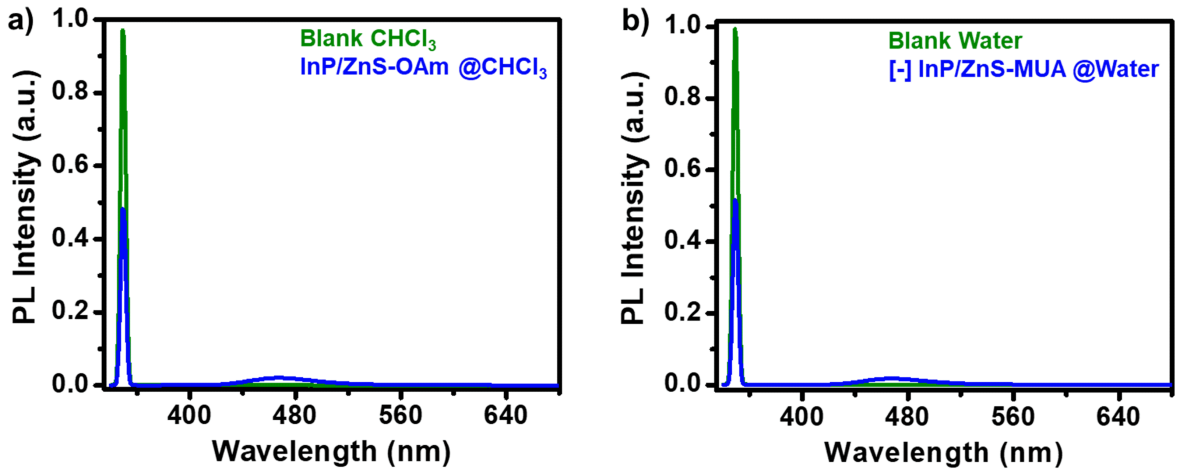

c)

System	Blank (Scattering)	Blank (PL)	QD (Scattering)	QD (PL)	Absolute QY $\left(\frac{\Delta PL}{\Delta Scattering} * 100\right)$
InP/ZnS-OAm	4.74 x 10^6	1.62 x 10^5	3.10 x 10^6	1.09 x 10^6	~56.50
[-] InP/ZnS-MUA	4.83 x 10^6	1.48 x 10^5	3.30 x 10^6	8.63 x 10^5	~46.80

Fig. S3 Absolute PL quantum yield (QY_A) measurements for pure-blue emitting InP/ZnS QDs in a) in $CHCl_3$ and b) water, under excitation at 350 nm. c) Table for the determination of absolute QY in $CHCl_3$ and water.

Zeta Potential and DLS Studies of Water Stable Pure-blue Emitting InP/ZnS QDs:

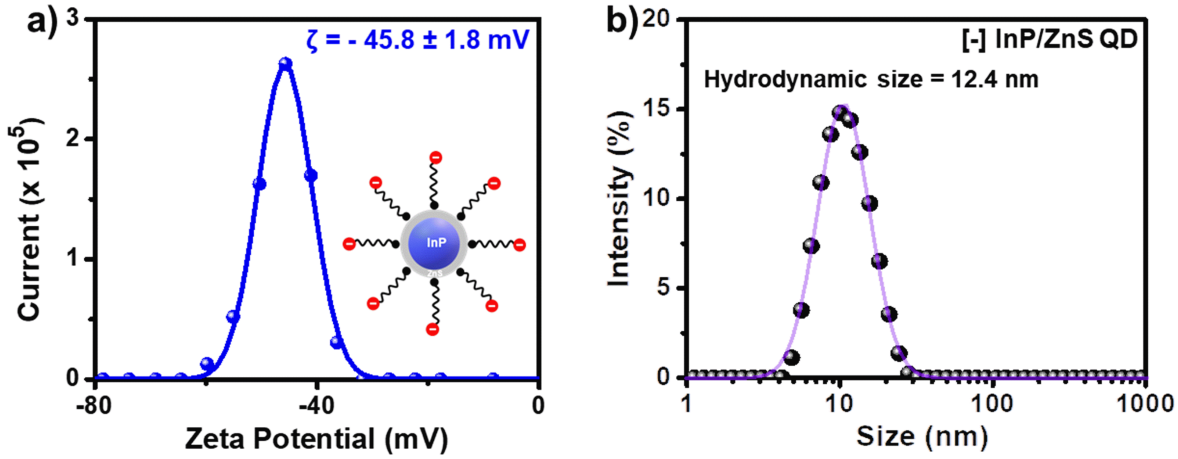

Fig. S4 Representative (a) zeta potential (ζ) and (b) dynamic light scattering (DLS) plots of [-] InP/ZnS QDs. The error was estimated from three different measurements on three different samples.

FTIR Studies of Pure-Blue Emitting InP/ZnS QDs Before and After the Place Exchange:

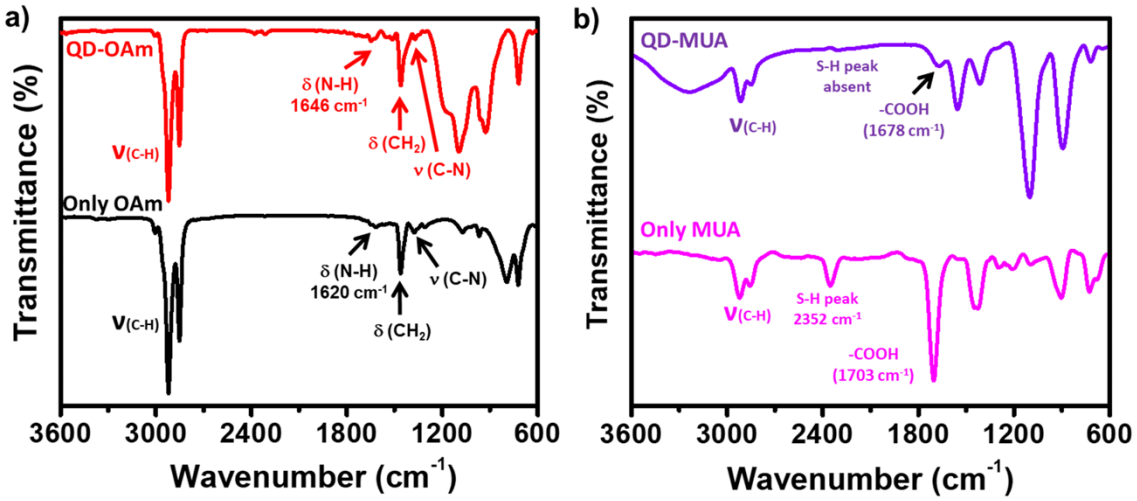

Fig. S5 FTIR spectra of (a) OAm ligand (black) and OAm capped InP/ZnS QD (red), (b) [-] MUA ligand (magenta) and [-] InP/ZnS QD (violet).

Table S1: Assignment of major IR peaks for OAm and OAm capped InP/ZnS QD.[5]

Samples	Major peaks observed	Peak assignments
OAm ligand	2852 cm^{-1} and 2920 cm^{-1}	$–CH_2$ and $–CH_3$ symmetric and asymmetric stretching frequency, respectively.[5]
	1620 cm^{-1}	N-H bending.[5]
	1460 cm^{-1}	CH_2 bending.[5]
	1377 cm^{-1}	C-N stretching.[5]
OAm capped InP/ZnS QD	All the above-mentioned characteristic peaks for OAm ligands were observed.	The N–H bending peak was blue shifted to 1646 cm^{-1}, confirming the binding of OAm ligands on the QD surface via $–NH_2$ group.[5]

Table S2: Assignment of major IR peaks for MUA and MUA capped InP/ZnS QDs.

Samples	Major peaks observed	Peak assignments
MUA ligand	2352 cm^{-1}	S–H stretching.[6]
	1703 cm^{-1}	Carbonyl stretching frequency of carboxyl group.[6]
	2849 cm^{-1} and 2915 cm^{-1}	$–CH_2$ and $–CH_3$ symmetric and asymmetric stretching frequency, respectively.[6]
MUA capped InP/ZnS QD	All the characteristic peaks for MUA ligand, except S-H peak, were observed	The absence of S–H stretching frequency confirms the binding MUA ligand on the surface of QD via the thiol group. There is a red shift in carbonyl stretching frequency because of the deprotonation of the acid group.[6]

NMR Studies of Pure-Blue Emitting InP/ZnS QDs Before and After the Place Exchange:

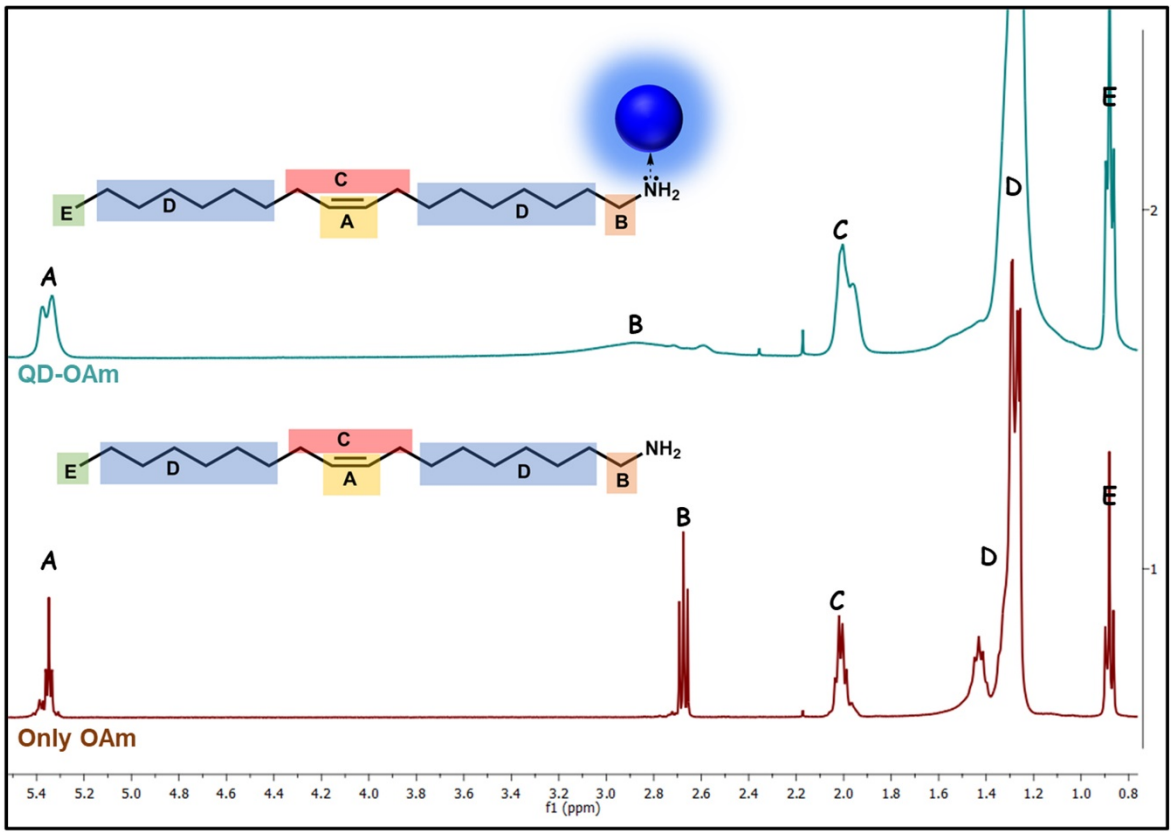

Fig. S6 ^{1}H NMR spectra of OAm ligand (wine red) and OAm capped InP/ZnS QD (Cyan) in $CDCl_3$. For only OAm molecule, ^{1}H NMR (400 MHz, $CDCl_3$) δ 5.41 – 5.31 (m, 1H), 2.67 (t, J = 7.0 Hz, 1H), 2.07 – 1.92 (m, 2H), 1.46 – 1.26 (m, 14H), 0.88 (t, J = 6.8 Hz, 2H).

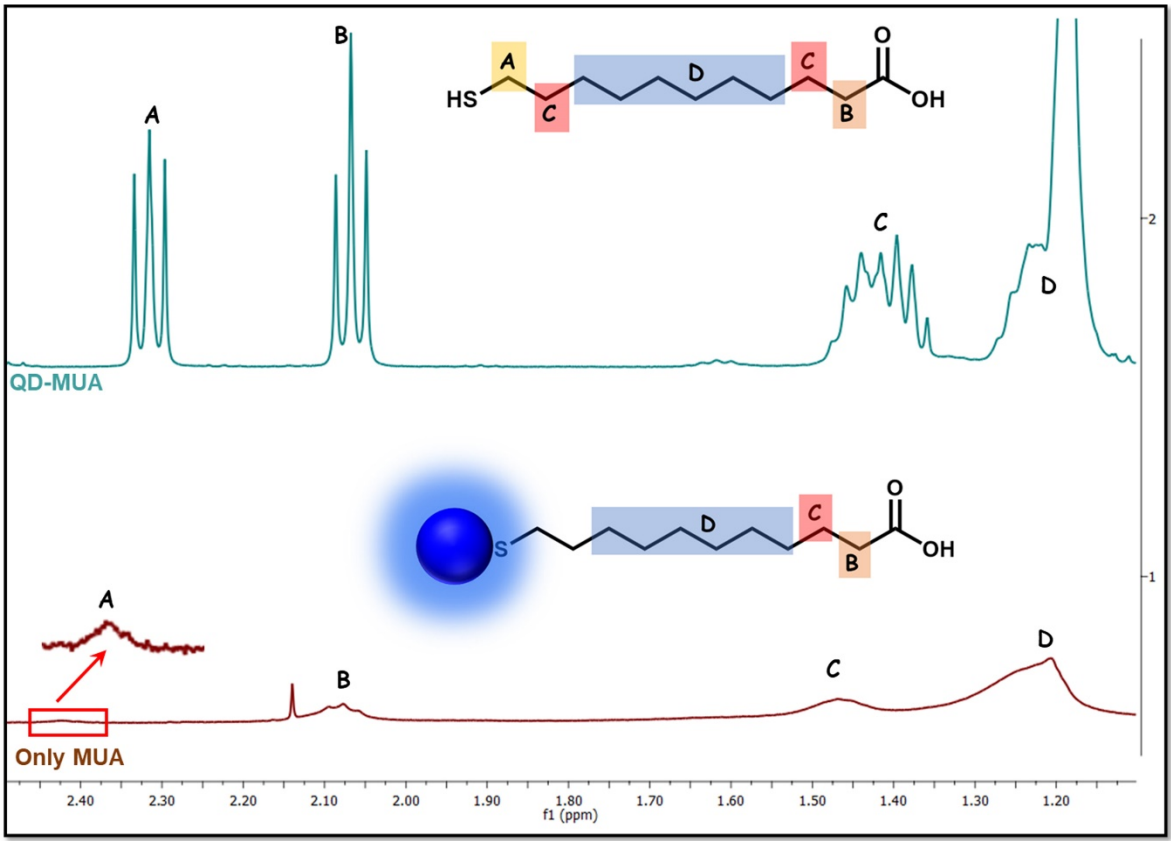

Fig. S7 ^{1}H NMR spectra of MUA ligand (cyan) and MUA capped InP/ZnS QD (wine red) in basic D_2O. For only MUA molecule, ^{1}H NMR (400 MHz, D_2O) δ 2.32 (t, 1H), 2.07 (t, J = 7.5 Hz, 1H), 1.46 – 1.36 (m, 2H), 1.24 – 1.17 (m, 6H).

We observed broad signals corresponding to the characteristic's peaks of OAm and MUA ligands for QD samples. Additionally, the peaks are getting blue shifted. The lack of any fine structure and observed blue shift indicates that the transversal interproton dipolar relaxation process becomes efficient through restricted rotational mobility of ligands when bound to the surface of QDs.[7-9] Therefore, all the ligands are attached to the InP/ZnS QD surface and there are no free ligands present in the solution.[7] This resonance broadening became more pronounced for the protons closer to the QDs surface and decreases as the distance increases from the QD surface (proton A, C and E in OAm capped InP/ZnS QD).

Thus, the phase transfer, IR, and NMR studies confirm the successful ligand exchange of OAm with MUA ligands on the surface of pure-blue emitting InP/ZnS QDs.

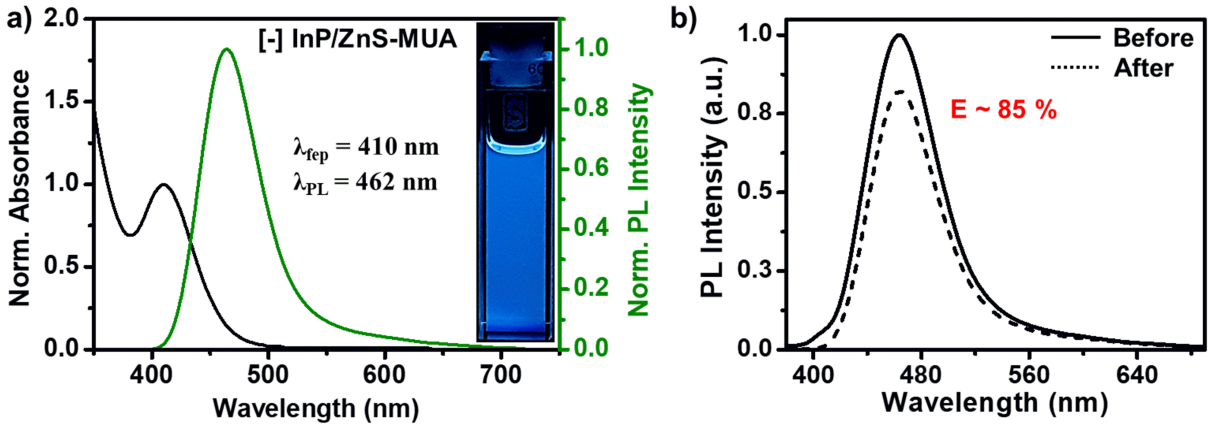

Fig. S8 The normalized UV-vis absorption and steady-state PL spectra of pure-blue emitting InP/ZnS QD in water. The wavelength of excitation was 370 nm. The insert shows the optical photograph of pure-blue emitting InP/ZnS QDs in water under UV excitation (~365 nm). b) The unnormalized PL spectra of InP/ZnS QDs before (solid) and after (dotted) the place exchange reaction, confirming ~85 % of PL retention.

A negligible change in absorption and photoluminescence spectra were observed after the place exchange reaction.

Lifetime Studies:

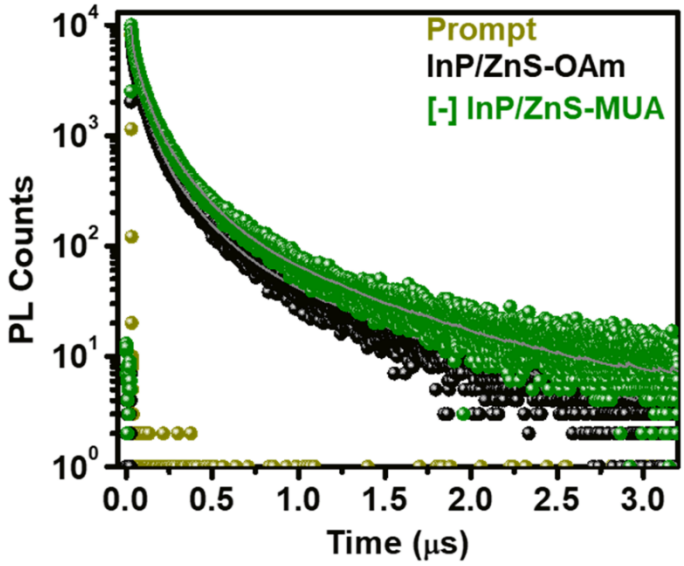

Fig. S9 PL decay profiles of OAm (black) and [-] MUA (olive green) capped pure-blue emitting InP/ZnS QDs. The wavelength of excitation was 370 nm.

Table S3. PL decay analysis of pure-blue emitting InP/ZnS QDs before and after surface functionalization with MUA ligands, in a time window of 3.2 µs.

System	τ_1 (ns)	α_1	τ_2 (ns)	α_2	τ_3 (ns)	α_3	τ_4 (ns)	α_4	$\tau_{avg.}$ (ns)	χ^2
InP/ZnS-OAm	4.21	0.47	46.46	0.37	143.61	0.14	585.15	0.02	206.80	1.14
	f_1 = 0.04		f_2 = 0.34		f_3 = 0.39		f_4 = 0.23			
[-] InP/ZnS-MUA	8.98	0.46	58.42	0.37	167.09	0.15	629.70	0.02	211.63	1.12
	f_1 = 0.06		f_2 = 0.34		f_3 = 0.39		f_4 = 0.21			

Photostability Under UV Irradiation:

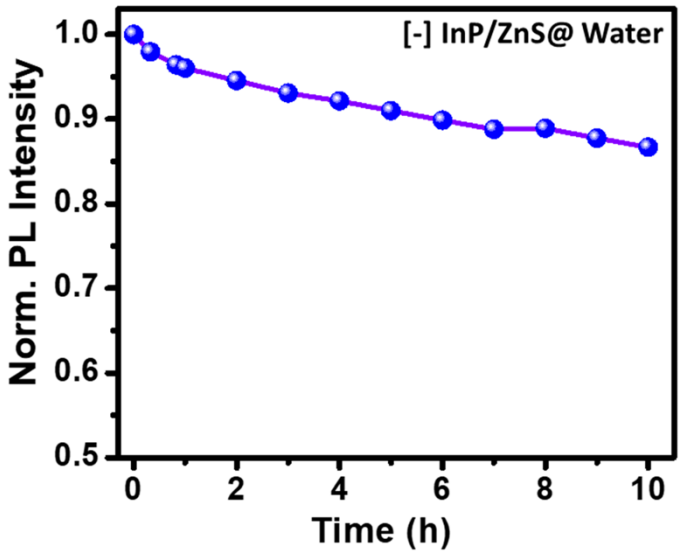

Fig. S10 A plot showing the long-term PL stability of [-] InP/ZnS QDs, under continuous irradiation with ~365 nm UV light for ~10 h (the power measured at the cuvette wall was ~6.2 mW/cm^2).

HRTEM Analysis:

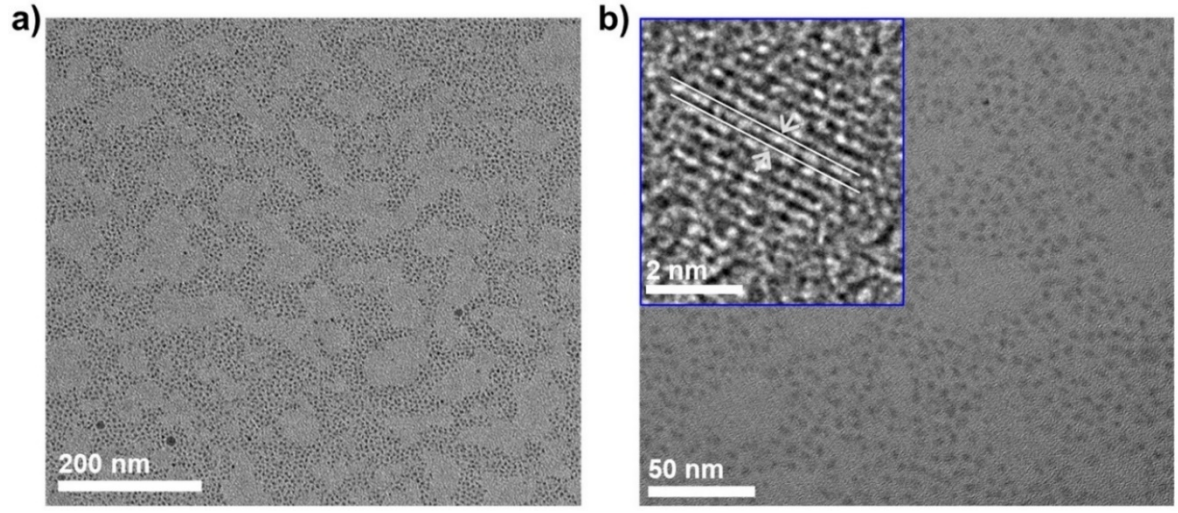

Fig. S11 High resolution transmission electron microscopy (HRTEM) analysis of pure-blue emitting [-] InP/ZnS QDs. Representative large area TEM images at resolution of (a) 200 nm, and (b) 100 nm,

showing the uniformity in size and shape distribution. The inset of (b) shows the lattice fringes in single [-] InP/ZnS QD.

Powder XRD Analysis:

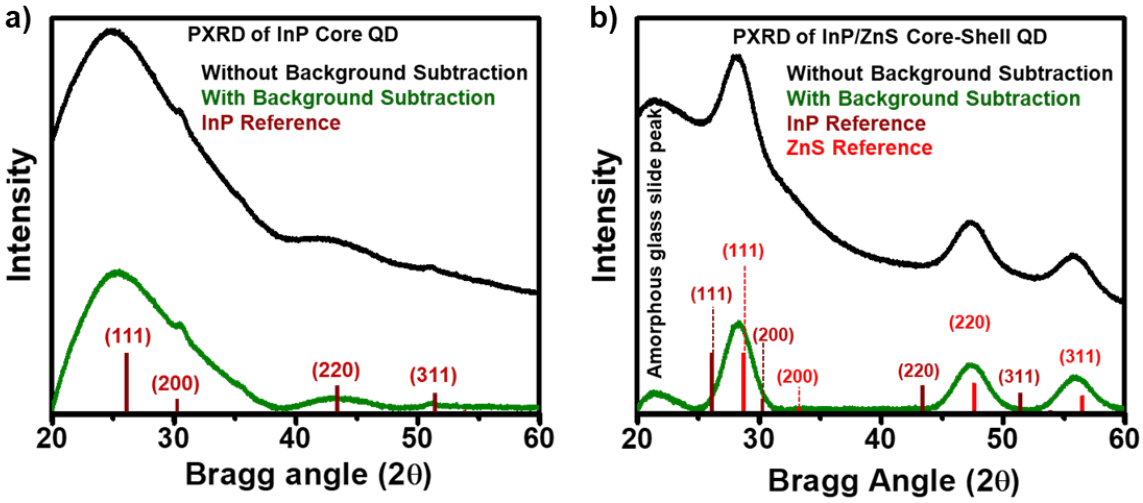

c)

System	(111) plane	(220) plane	(311) plane	Average size
InP core QD	---	L = 5.02° 2θ = 43.47° D = 1.78 nm	---	1.79 nm
InP/ZnS core-shell QD	L = 2.63° 2θ = 28.28° D = 3.26 nm	L = 2.65° 2θ = 47.40° D = 3.42 nm	L = 2.56° 2θ = 55.94° D = 3.66 nm	3.45 nm

Fig. S12 Powder X-ray diffraction (PXRD) patterns of (a) InP-core and (b) InP/ZnS core-shell QDs without (black) and with (olive) background substraction. Comparison of PXRD patterns of QDs with bulk InP (wine-solid) and ZnS (red-solid) reference reveals the presence of zinc blend phase in InP-core and InP/ZnS core-shell QD.[10] The broadness of the first peak (around 2θ = 25 degrees) in InP-core is due to the combination of signal from (111) and (200) planes of zinc blend phase and the underlying amorphous glass slide.[10-11] (c) Table for the calculation of diameter of InP-core and InP/ZnS core-shell QDs from Scherrer equation.

The crystallite size of the core InP and core-shell InP/ZnS QDs was determined from PXRD peaks using Scherrer equation.[12]

$$D = \frac{k\lambda}{\beta \cos\theta} \quad \text{... (4)}$$

Where, D = Crystallite size

k = Scherrer constant, is typically considered to be 0.94 for spherical particles

λ = Wavelength of Cu k_α X-ray = 1.5406 Å

β = FWHM of the PXRD peak in radian.

θ = Bragg angle

The Scherrer equation quantitatively describes the broadening of a peak at a particular angle (θ), as it relates the crystalline domain size (D) to the width of the peak (β). By using the above equation 4, the crystallite size of the InP-core and InP/ZnS core-shell QDs was determined to 1.8 ± 0.1 nm and 3.5 ± 0.2 nm, respectively.

XPS Studies of Pure-Blue Emitting InP/ZnS QDs Before and After the Place Exchange:

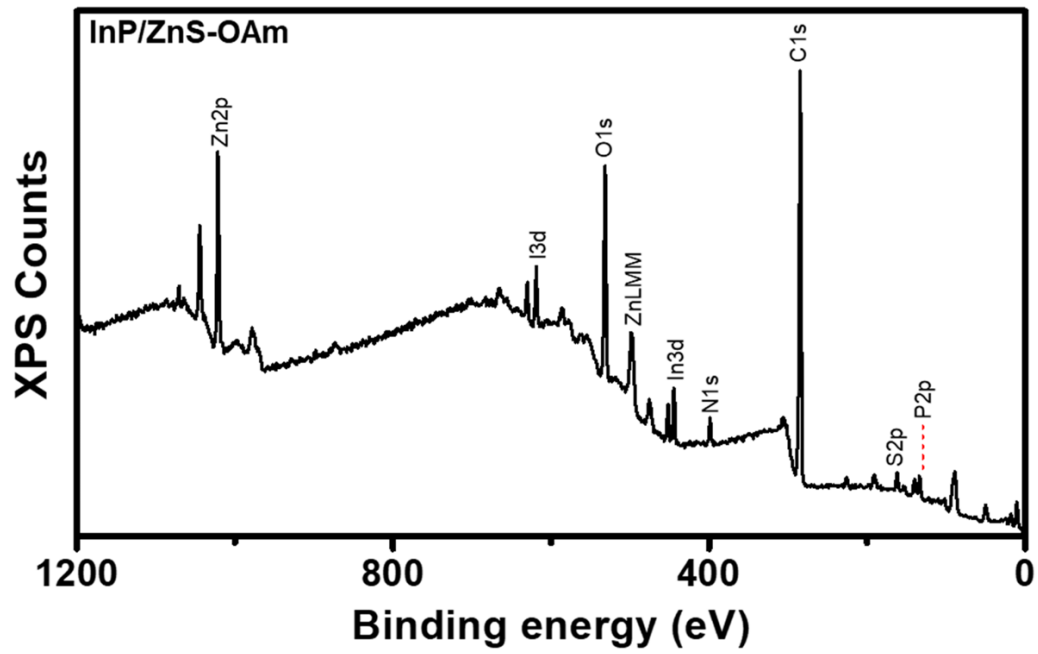

Fig. S13 XPS survey spectra of InP/ZnS-OAm QDs. The characteristics peaks corresponding to all the major elements are properly assigned: In3d, P2p, Zn**2**p, Zn3s, S2p, C1s, N1s, O1s.

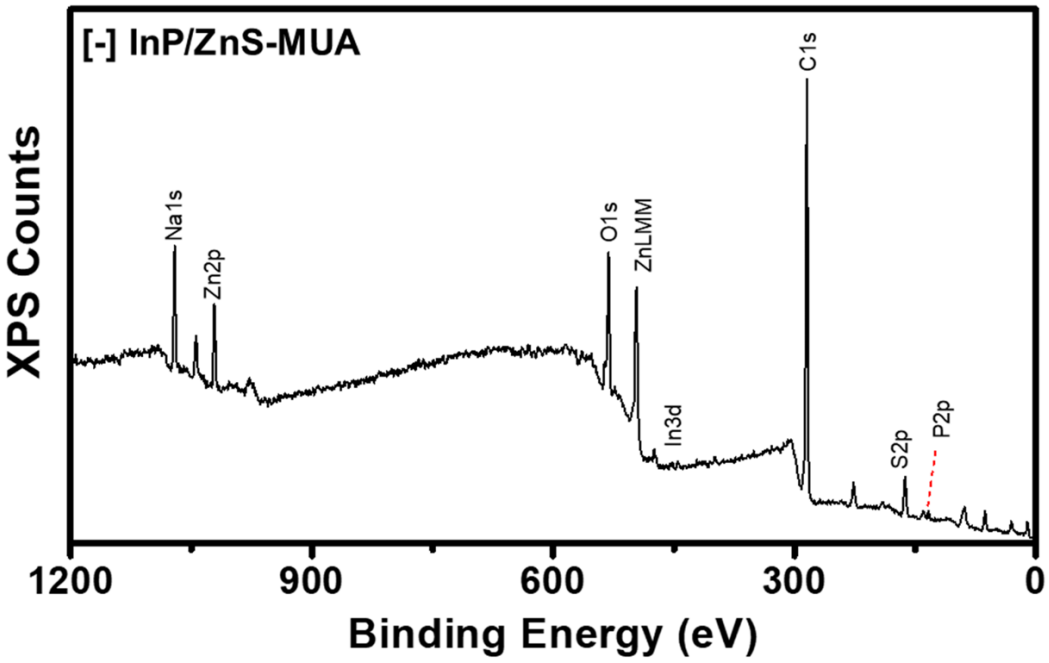

Fig. S14 XPS survey spectra of [-] InP/ZnS-MUA QDs. The characteristics peaks corresponding to all the major elements are properly assigned: In3d, P2p, Zn2p, Zn3s, S2p, C1s, N1s, O1s.

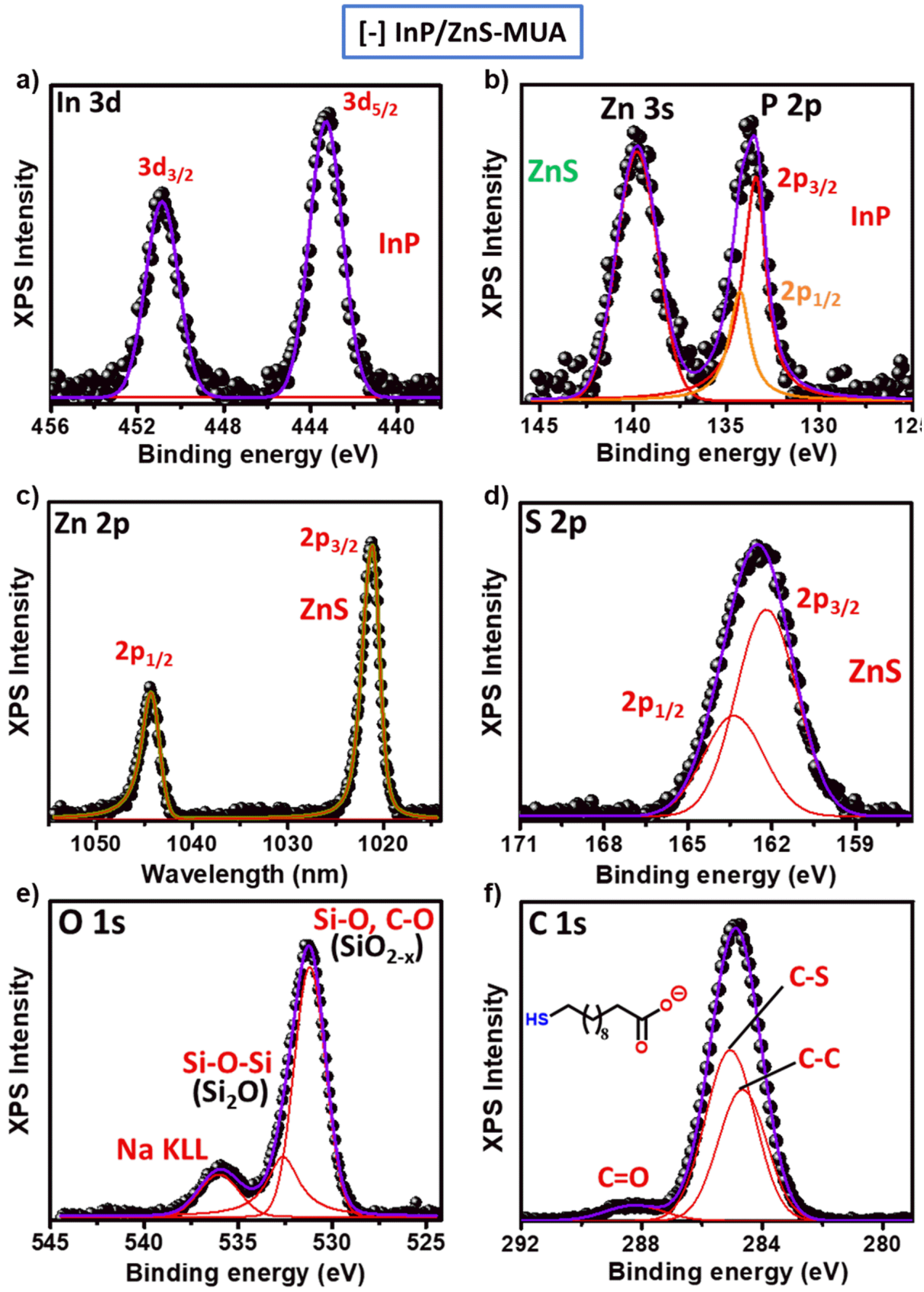

Fig. S15 Analysis of X-ray photoelectron spectrum of [-] InP/ZnS-MUA QDs: (a) In 3d spectrum; (b) P 2p spectrum, Zn 3s spectrum; (c) Zn 2p spectrum; (d) S 2p spectrum; (e) O 1s spectrum; and (f) C 1s spectrum.

A detailed elemental analysis of [-] InP/ZnS QD was performed using of X-ray photoelectron spectroscopy (XPS). The In 3d, P 2p, Zn 2p, Zn 3s, and S 2p core peaks as well as the peaks for the surface ligands O 1s, C 1s and Na KLL auger are present in the system (Fig. S14).[13-14] For the analysis, the charge correction for the all the spectral peaks was performed according to the carbon-1s standard peak (284.6 eV).

For, [-] InP/ZnS-MUA QD, the In 3d and P 2p spectrum exhibits one doublet corresponding to In-P bond.[13,15-16] The doublet for In was located at 443.26 eV ($3d_{5/2}$) and 450.86 eV ($3d_{3/2}$), respectively (spin-orbit splitting of 7.6 eV between $3d_{5/2}$ and $3d_{3/2}$). The doublet for P appears at 133.44 eV ($2p_{3/2}$) and 134.34 eV ($2p_{1/2}$), respectively (spin-orbit splitting of 0.9 eV between $2p_{3/2}$ and $2p_{1/2}$). The presence of single doublet for In 3d and P 2p indicates the absence of any oxidised $InPO_x$ layer at the interface of core and shell materials.[16] Further, the analysis of O 1s spectrum confirms the absence of oxide layer, instead, there was a presence of Na KLL auger peak at 536.04 eV, justifying the presences of deprotonated MUA ligand on the QD surface. The Zn 2p XPS exhibit two peaks located at 1021.14 eV ($2p_{3/2}$) and 1044.34 eV ($2p_{1/2}$) (spin-orbit splitting of 23.2 eV between $2p_{3/2}$ and $2p_{1/2}$), assigned to the ZnS shell.[15] A single Zn 3s peak was also observed at 139.74 eV. The S 2p spectrum showed one doublet located at 162.24 eV ($2p_{3/2}$) and 163.34 eV ($2p_{1/2}$) (spin-orbit splitting of 1.1 eV between $2p_{3/2}$ and $2p_{1/2}$). This decrease in spin-orbit splitting can be attributed to the combined effect of ionic metal-sulphur and covalent C-S bond present in the system.[16] Finally, the characteristic peaks for the surface MUA ligands were analysed with C1s spectrum. The C 1s spectrum showed three peak corresponds to C-C (284.64 eV), C-S (285.04 eV) and C=O (288.24 eV) bond for the MUA ligand.[16-18]

Table S4: Summary of XPS results for [-] InP/ZnS-MUA QDs.

Entry	Binding energy (eV)	Chemical states	Spin-orbit splitting (eV)
In 3d	443.26 ($3d_{5/2}$)	InP	7.6
	450.86 ($3d_{3/2}$)		
P 2p	133.44 ($2p_{3/2}$)	InP	0.9
	134.34 ($2p_{1/2}$)		
Zn 3s	139.74	ZnS	---
Zn 2p	1021.14 ($2p_{3/2}$)	ZnS	23.2
	1044.34 ($2p_{1/2}$)		
S 2p	162.24 ($2p_{3/2}$)	ZnS	1.1
	163.34 ($2p_{1/2}$)		

O1s & Na Auger	531.24	Si-O (SiO_{2-x}), C-O	---
	532.64	Si-O-Si (SiO_2)	---
	536.04 Na KLL	Na KLL Auger	---
C 1s	284.64	C-C	---
	285.04	C-S	---
	288.24	C=O	---

EDAX Analysis:

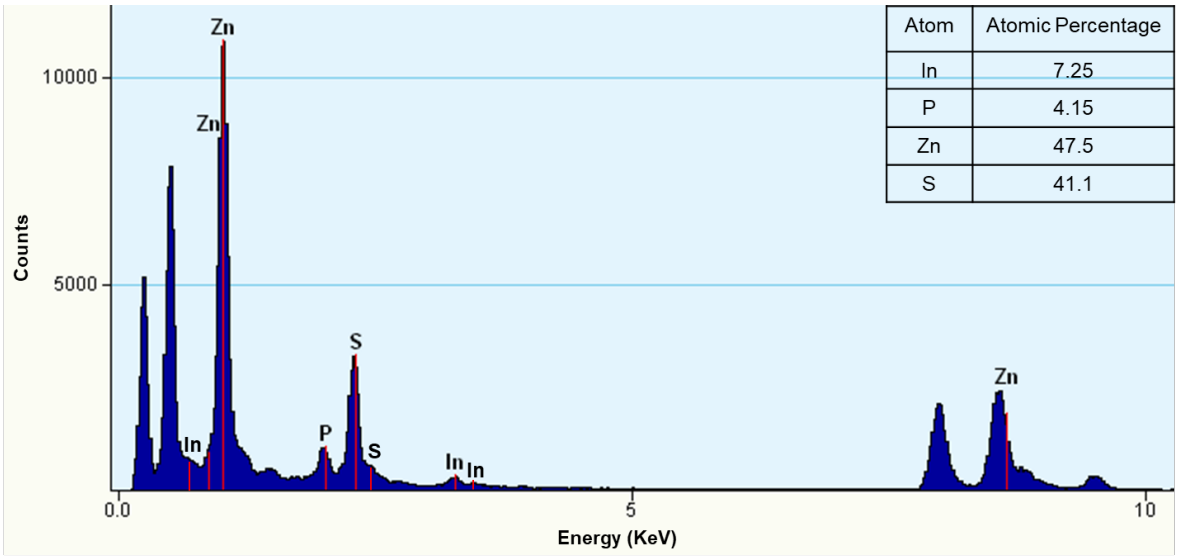

Fig. S16 EDAX spectrum of [-] InP/ZnS QDs, taken during the HRTEM measurement. The inset shows the atomic percentages of all the major components in [-] InP/ZnS QDs: In, P, Zn and S.

Cyclic Voltammetry Studies and Band Measurements:

The onset oxidation potential for pure-blue emitting InP/ZnS QDs was estimated to be +1.62 V, relative to the Ag/Ag^+ reference electrode. The valence band edge energy level was determined by following the equation.[19]

$$E_{VB} = -I_P = -(eE_{Ox} + E_{Ref})eV \quad \text{... (5)}$$

The valence band position was estimated to be -6.33 eV *vs* vacuum. The conduction band (CB) position was measured from the difference between the valence band position (VB, obtained from CV measurement) and band gap of the QD calculated from the Tauc plot. The CB position is at -3.63 eV *vs* vacuum.

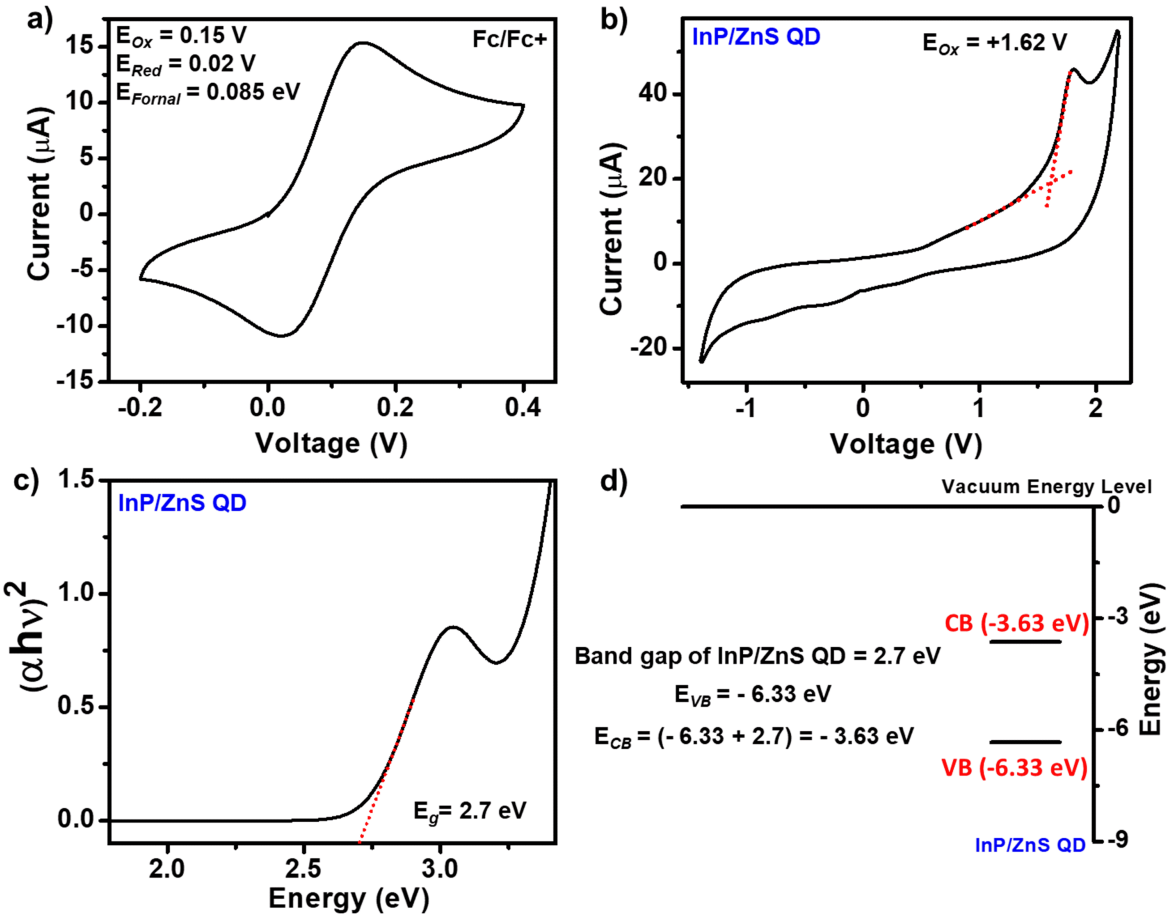

Fig. S17 Determination of band positions for the pure-blue emitting InP/ZnS QD. Cyclic voltammograms for (a) ferrocene/ferrocenium couple, as internal standard and (b) InP/ZnS QD in acetonitrile solvent, at a scan rate of 30 mV/s. The measurements for QDs were performed via dip-coating of QDs over the glassy carbon, followed by drying under vacuum to remove the solvent. The measured relative reference electrode potential, E_{ref}, is 4.71 eV. (c) The Tauc plot for InP/ZnS QD. (d) Relative band positions for InP/ZnS QD, with respect to vacuum.

Determination of Molar-Extinction Coefficient of InP/ZnS QDs:

The particle concentration of InP/ZnS QDs and the corresponding molar extinction co-efficient (0.2519 x 10^5 $M^{-1}cm^{-1}$ at 410 nm) were estimated using ICP-MS analysis combined with PXRD, TEM and UV-vis absorption spectrum. Details are provided below.

Size of the particle, *d* (from PXRD analysis) = 17.8 Å

Lattice constant of InP, a[20] = 5.83 Å

Note: InP crystallizes in cubic zinc blende structure with a lattice constant (*a*) of 5.83 Å with 8 atoms in unit cell (4 In and 4P)

Volume of the unit cell, $V_{unit\ cell}$ = a^3

Total number of atoms in a nanocrystal, A $= \frac{4}{3}\pi\left(\frac{d}{2}\right)^3 * \frac{8}{V_{unit\ cell}} = 119$

Let's consider that the mass % of In and P is C_{In} and C_P, respectively.

Concentration of InP/ZnS nanocrystals[21], $C_{InP/ZnS}$ $= \frac{1}{A}\left(\frac{C_{In}}{M_{In}} + \frac{C_P}{M_P}\right)$ **... (6)**

M is the molar mass.

N.B. From EDAX analysis, the obtained ratio of In to P was 1:0.56.

Table S5: Concentration values of In and P obtained from ICP-MS analysis, and the corresponding concentration of InP/ZnS QDs (determined from equation 6).

Conc. of In (C_{In}) (ppb)	**Conc. of P (C_P) (ppb)**	**Conc. of InP/ZnS QDs ($C_{InP/ZnS}$), nM (Form Eq.1)**
2.5	1.4	0.56
3.4	1.9	0.75
4.3	2.4	0.94
4.9	2.7	1.09
5.8	3.2	1.27
6.5	3.6	1.45
7.3	4.1	1.62
8.1	4.5	1.78

The molar extinction co-efficient (ε) was determined using the Beer-Lambert law.[21]

$$\boldsymbol{A = \varepsilon \cdot c \cdot l} \quad \textbf{... (7)}$$

Where, A= Absorbance or optical density

ε = Absorption coefficient or molar extinction coefficient ($M^{-1}cm^{-1}$)

C = Concentration of the solution (mol L^{-1})

l = Optical path length = 1 cm

The slope of optical density vs concentration plot will provide the molar extinction co-efficient (ε), which was estimated to be 0.2519 x 10^5 $M^{-1}cm^{-1}$.

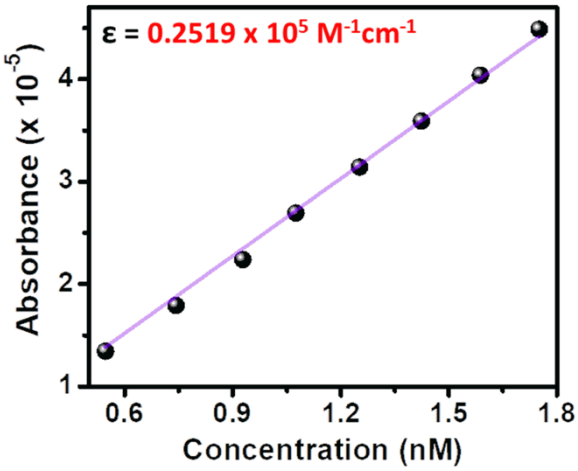

Fig. S18 A plot of optical density vs concentration of InP/ZnS QDs.

Reason for unusually high photophysical performance of blue-emitting InP/ZnS QDs:

In our study, a fine control over the shell growth and thickness led to the formation of high-quality pure-blue emitting InP/ZnS QDs. In general, the InP core is overcoated with a ZnS shell via hot-injection techniques. Important point to be mentioned here is that the high temperature crystallization process continues even during the cooling process.[22] With this thought in mind, instead of cooling the reaction system after the successful formation of InP core, a quick and direct injection of Zn- and S-precursors was done at high temperature and inert atmosphere. In a typical procedure, after the successful synthesis of InP core at 200 ^{0}C, Zn-precursor dissolved in octadecene (ODE) and dodecanethiol (DDT, S-precursor) was added to the reaction mixture. Then, the reaction temperature was increased to 300 ^{0}C and allowed to react for 45 min. Here, an optimized Zn- and S-precursor amount provides a fine control over the thickness of the ZnS shell. This allowed us to restrict the growth of the ZnS shell to ~3 monolayers. The consequence of having a small InP core size and a thin ZnS shell is as follows. The energy difference between small InP core and ZnS shell is not significant enough to form a typical type-I core-shell QDs. Instead, they form a quasi-type-II core-shell QDs.[23] As the shell thickness is less, the excitons will be mainly confined within the InP core.[23-24] As a result, the PL QY will be high and the PL maxima will be centered around the band edge emission of the core QDs (~462 nm in the present study). A thicker shell will lead to the delocalization of the electron wave function to the shell, which compromises the photophysical properties of the QDs.[24]

Section 3: Stability and Bioimaging with Pure-Blue Emitting QDs

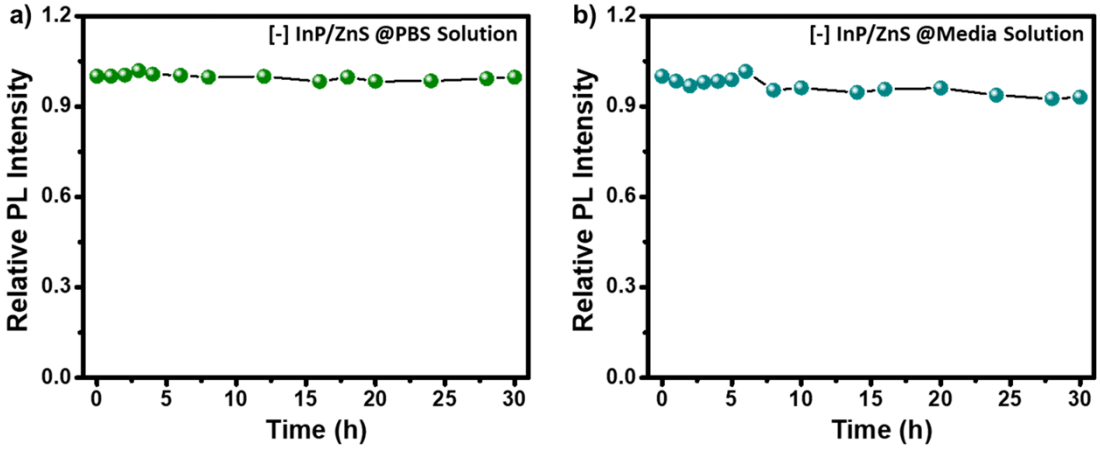

Fig. S19 The plots showing the PL stability of [-] InP/ZnS QDs in (a) PBS buffer and (b) biological media solution (5 % FBS in media solution).

Cell Viability Studies:

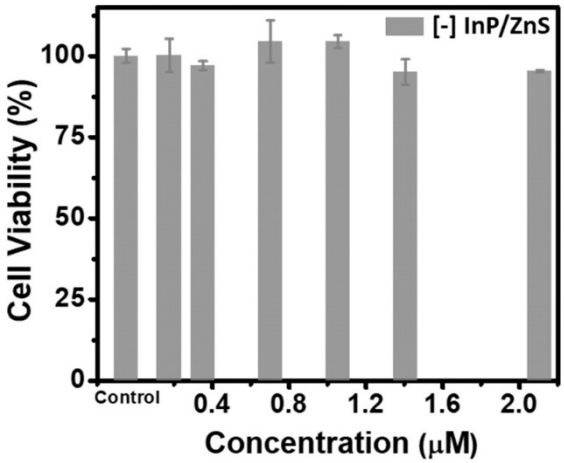

Fig. S20 MTT assay with [-] InP/ZnS QDs, showed ~95 % viability of Hella cell with 120 µg/mL QD (~2.1 µM).

Bioimaging:

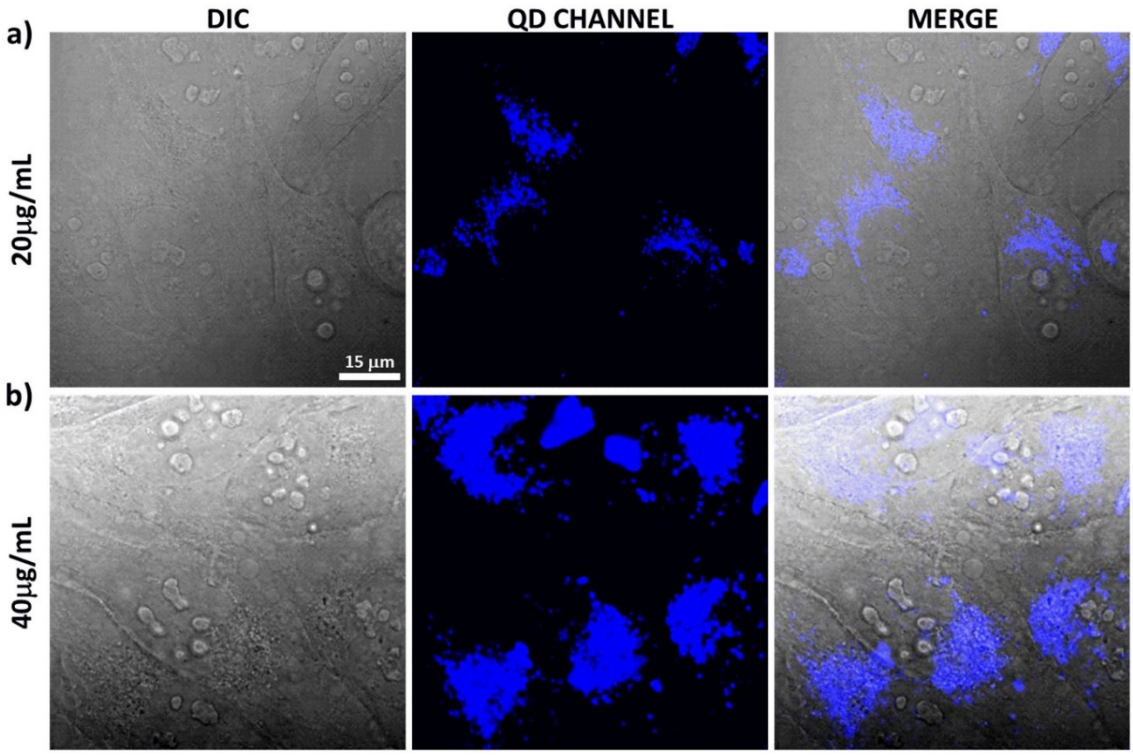

Fig. S21 Concentration optimization for bio-imaging study. Luminescent confocal images of Hela cells internalized with (a) 20 µg/mL [-] InP/ZnS QDs (0.35 µM), and (a) 40 µg/mL [-] InP/ZnS QDs (0.70 µM) for ~7 h. The first and second column corresponds to phase contrast (DIC) image and the fluorescence image upon excitation with 405 nm laser source, respectively. The third column corresponds to the fluorescence image merged with DIC image.

Cellular Uptake Mechanism of [-] InP/ZnS QD:

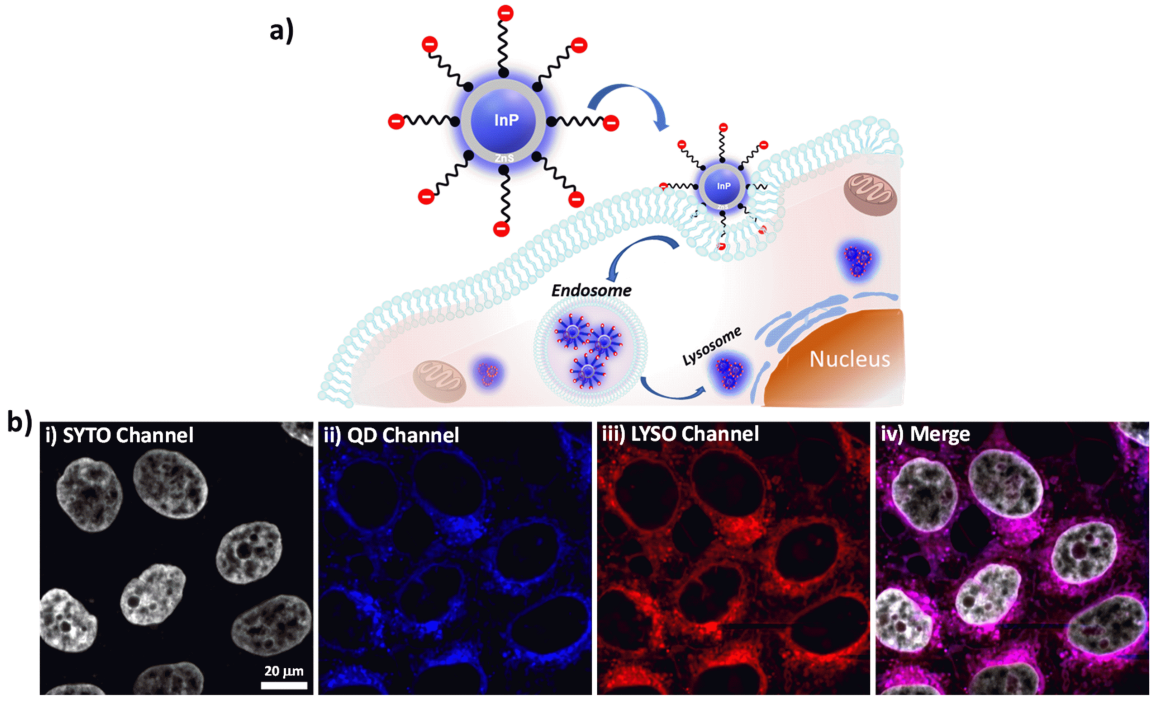

Fig. S22 Co-staining experiments for cellular uptake mechanism study. (a) A representative scheme showing the endocytosis of [-] InP/ZnS QDs inside the cells. (b) Nucleus staining with (i) syto-deep red dye, (ii) blue channel for quantum dot, (iii) co-staining with lysotracker DND 26 dye for marking the lysosomes of the cells, and (iv) merge image showing colocalization of [-] InP/ZnS QDs with lysotracker DND 26.

To track the incubation pathway, the nuclei and lysosome of [-] InP/ZnS QD treated cells were co-stained with SYTO-dye and lysotracker dye, respectively. Here, the red-color is coming only from lysosome of the cell as the lysotracker dye selectively stains these tiny acidic compartments of the cells over any other organelles. Interestingly, the blue-channel from QD emission exactly overlay with the red channel, as can be seen from the merge image. Thus, the [-] InP/ZnS are successfully taken inside the cells via an organized pathway of endocytosis as they are localized inside the lysosome of the cell.

Section 4: Background of Förster Resonance Energy Transfer (FRET) Formalism

The Förster resonance energy transfer (FRET) process is a non-radiative transfer of energy from an excited state donor to a ground state acceptor.[6,25] It is driven by the long-range dipole-dipole interaction, and thus is strongly dependent on the donor-acceptor distance. Also, it demands an appreciable spectral overlap between the emission of donor and absorption of acceptor fluorophores.

The rate of energy transfer between donor and acceptor at a distance r can be expressed as[25]

$$\boldsymbol{k_T(r) = \frac{B\Phi_D J(\lambda)}{\tau_D r^6} = \frac{1}{\tau_D}\left(\frac{R_0}{r}\right)^6} \quad \text{... (8)}$$

Where, R_0 is the Förster distance at which FRET efficiency is 50%, r is the distance between donor and acceptor, J(λ) is the spectral overlap integral between emission of donor and absorption of acceptor. Φ_D and τ_D are the PL quantum yield and lifetime of donor, respectively.

B is a constant that can be written as a function of refractive index of the medium η_D, Avogadro's number N_A and dipole orientation parameter κ_p:[26]

$$\boldsymbol{B = \frac{[9000(ln10)]\kappa_p^2}{128\pi^5\eta_D^4 N_A}} \quad \text{... (9)}$$

The orientation factor (κ_p) varies from 0 (for perpendicular alignment of the D-A dipoles) to 4 (for parallel orientation). The dynamic average value of k_p was assumed to be 2/3.[25,26]

Here, the Förster distance R_0 is given by[25]

$$R_0 = \left(B\phi_D J(\lambda)\right)^{1/6} = 0.2018\left(\frac{\phi_D \kappa_p^2 J(\lambda)}{\eta^4}\right)^{1/6} \text{ Å} \quad \text{... (10)}$$

Calculation of Spectral Overlap Integral:

The spectral overlap integral was estimated using the well-accepted equation, which takes account of the donor fluorescence and acceptor absorption properties, respectively.[25,26]

$$J(\lambda) = \int_0^\infty F_D(\lambda)\, \epsilon_A(\lambda)\, \lambda^4\, d\lambda \quad M^{-1}cm^{-1}nm^4 \quad \text{... (11)}$$

Where, $F_D(\lambda)$ is the normalized fluorescence intensity of donor at a particular wavelength (λ), ϵ_A is the molar extinction coefficient of the acceptor at a particular wavelength. Higher the value of $J(\lambda)$, better the probability for a donor-acceptor system to become an efficient FRET pair.

Calculation of Efficiency of FRET Process:

The efficiency of FRET can be calculated from steady-state emission and lifetime experiments.[25]

From steady-state PL quenching,

$$E = 1 - \frac{I_{DA}}{I_D} \quad \text{... (12)}$$

From lifetime quenching studies,

$$E = 1 - \frac{\tau_{DA}}{\tau_D} \quad \text{... (13)}$$

The F_{DA}, τ_{DA} are fluorescence intensity and lifetime of donor in presence of acceptor and F_D, τ_D are fluorescence intensity and lifetime of donor in absence of acceptor.

Also, the distance between donor and acceptor can be calculated from the efficiency using the following equation.

$$E = \frac{R_0^6}{R_0^6 + r^6} \quad \text{... (14)}$$

For non-covalently bonded donor-acceptor system, the critical concentration of acceptor (A_0) can be calculated from the Forster distance (R_0) of the system, by using the following equations.[25,27]

$$A_0 = \frac{3000}{2\pi^{3/2} N_A R_0^3} \quad \text{... (15)}$$

If R_0 is expressed in cm, the value of A_0 will be in mole/L, that is molarity (M).

The term A_0 represents the concentration at which the intramolecular energy transfer efficiency among the acceptors will be 76 %. Thus, when the acceptor concentration exceeds one hundredth of its critical concentration, possible intramolecular process will start to contribute.

Section 5: Resonance Energy Transfer Studies in Aqueous Medium

Steady-State Measurements

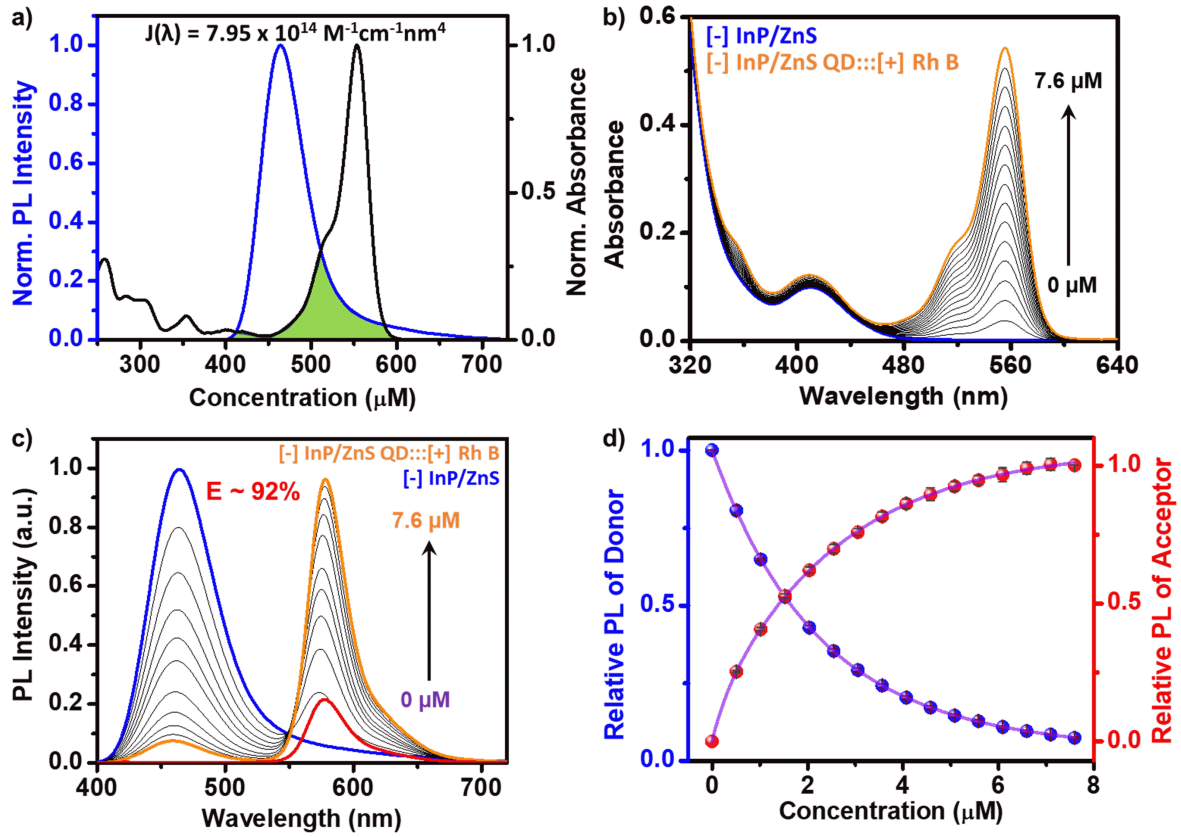

Fig. S23 FRET study between oppositely charged pure-blue emitting InP/ZnS QD and Rh B dye in water. (a) The spectral overlap integral between the PL of donor InP/ZnS QD and the absorption of acceptor Rh B dye. (b) Absorption and (c) PL spectral changes in pure-blue emitting InP/ZnS QD upon addition of increasing concentration of Rh B dye. The red spectrum in (c) indicates the PL intensity of 7.6 μM concentration of Rh B dye in absence of donor [-] InP/ZnS QD, when excited at 370 nm. (d) Plot showing the saturation of relative PL intensity of donor [-] InP/ZnS QDs and acceptor Rh B dye in [-] InP/ZnS:::Rh B system as a function of increasing concentration of Rh B dye.

Radius of Quenching Sphere and Perrin Formalism: A detailed Stern-Volmer analyses for [-] InP/ZnS QD:::Rh B complex in aqueous medium reveal a non-linear variation of relative PL intensity of [-] InP/ZnS QDs as a function of varying concertation of Rh B dye. In general,

the steady-state non-linear Stern-Volmer (I_0/I *vs* [Q]) indicates the presence of both static and dynamic components in the PL quenching. The exponential variation observed in relative PL can be treated within the framework of Perrin formalism, as shown below.[28-30]

$$\frac{I_0}{I} = e^{\alpha[Q]} = e^{\lambda} \quad \text{... (16)}$$

Where, the α represents the quenching constant, [Q] is concentration of acceptor and λ is the number of acceptors in the quenching sphere. Therefore, the plot of "ln (I_0/I) *vs* [Q]" will show a linear relationship and from the slope the quenching constant (α) can be determined. In the Perrin formalism, the quenching constant vary proportionally with the quenching volume (V) of the D-A system, as described below.

$$\alpha = \frac{N_A V}{1000} \quad \text{... (17)}$$

Where,

$$V = \frac{4}{3} r_q^3 \quad \text{... (18)}$$

r_q is quenching radius for the donor-acceptor system and N_A is the Avogadro number (6.023 x 10^{23} mol^{-1}).

The quenching constant (α) for [-] InP/ZnS QD:::Rh B donor-acceptor system was estimated to be ~4 x 10^5 M^{-1}. Thus, from the α value obtained, the calculated quenching volume and radius was estimated to be ~6.62 x 10^{-16} cm^3 and 54.1 nm, respectively. Here, the idea of quenching volume suggests an active volume or "sphere of action" surrounding the excited state QDs. Instantaneous quenching will occur in a randomly distributed system when a quencher happens to be resided within the sphere of action of volume "V".

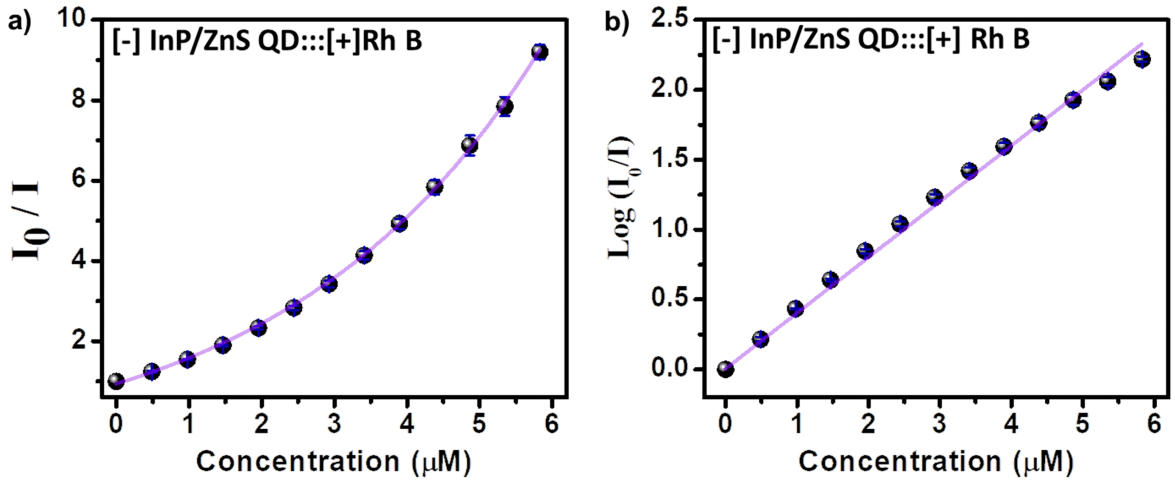

Fig. S24 Stern-Volmer analysis treated within the framework of Perrin formalism. (a) Relative PL intensity (I_0/I) of [-] InP/ZnS QD as a function of Rh B concentration. (b) The plot for $\ln(I_0/I)$ *vs* concertation of acceptor Rh B dye.

Photoluminescence Excitation Study:

Detailed PL excitation (PLE) studies were performed at the donor (~462 nm) and acceptor (~575 nm) emission wavelengths to monitor the excited state dynamics of FRET process. Here, the PL intensity collected at the donor emission wavelength (~462 nm) in [-] InP/ZnS QD:::Rh B dye donor-acceptor system was lower in the region of QD exciton and lower wavelengths, compared to only [-] InP/ZnS QD. However, the PL intensity collected at the acceptor emission wavelength (~575 nm) showed an enhancement at the QD exciton band in [-] InP/ZnS QD:::Rh B complex, compared to only Rh B dye. This confirms that the light absorbed by the QD donor is transferring to the Rh B dye acceptor, resulting in the emission from the acceptor.[6]

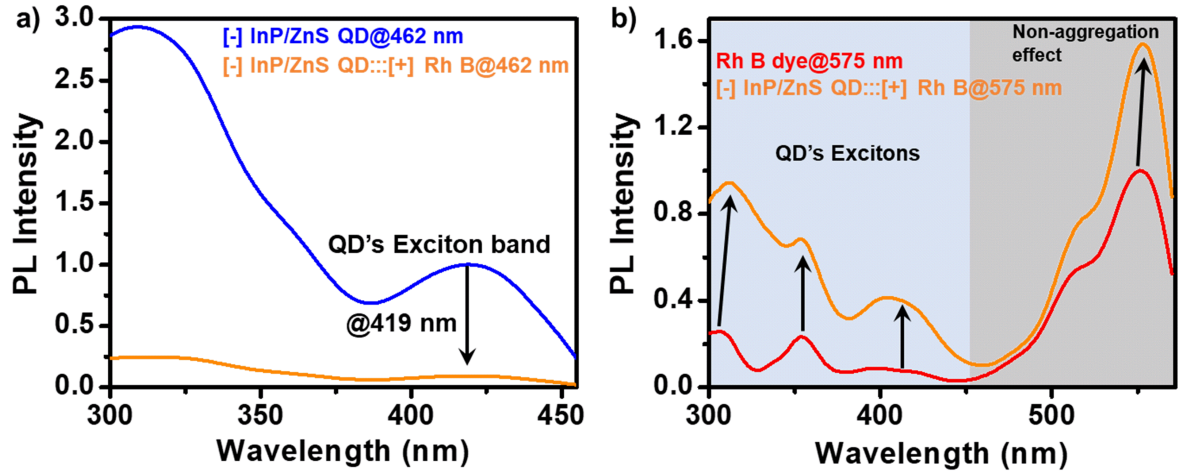

Fig. S25 PLE study for [-] InP/ZnS QD:::Rh B dye complex in water. (a) The excitation spectra of donor [-] InP/ZnS QD in presence (orange) and absence (blue) of acceptor Rh B dye, collected at 462 nm (emission wavelength of donor QD). (b) The excitation spectra of Rh B dye in presence (orange) and absence (red) of donor [-] InP/ZnS QD, collected at 575 nm (emission wavelength of acceptor Rh B dye).

Proof of Electrostatically Driven FRET:

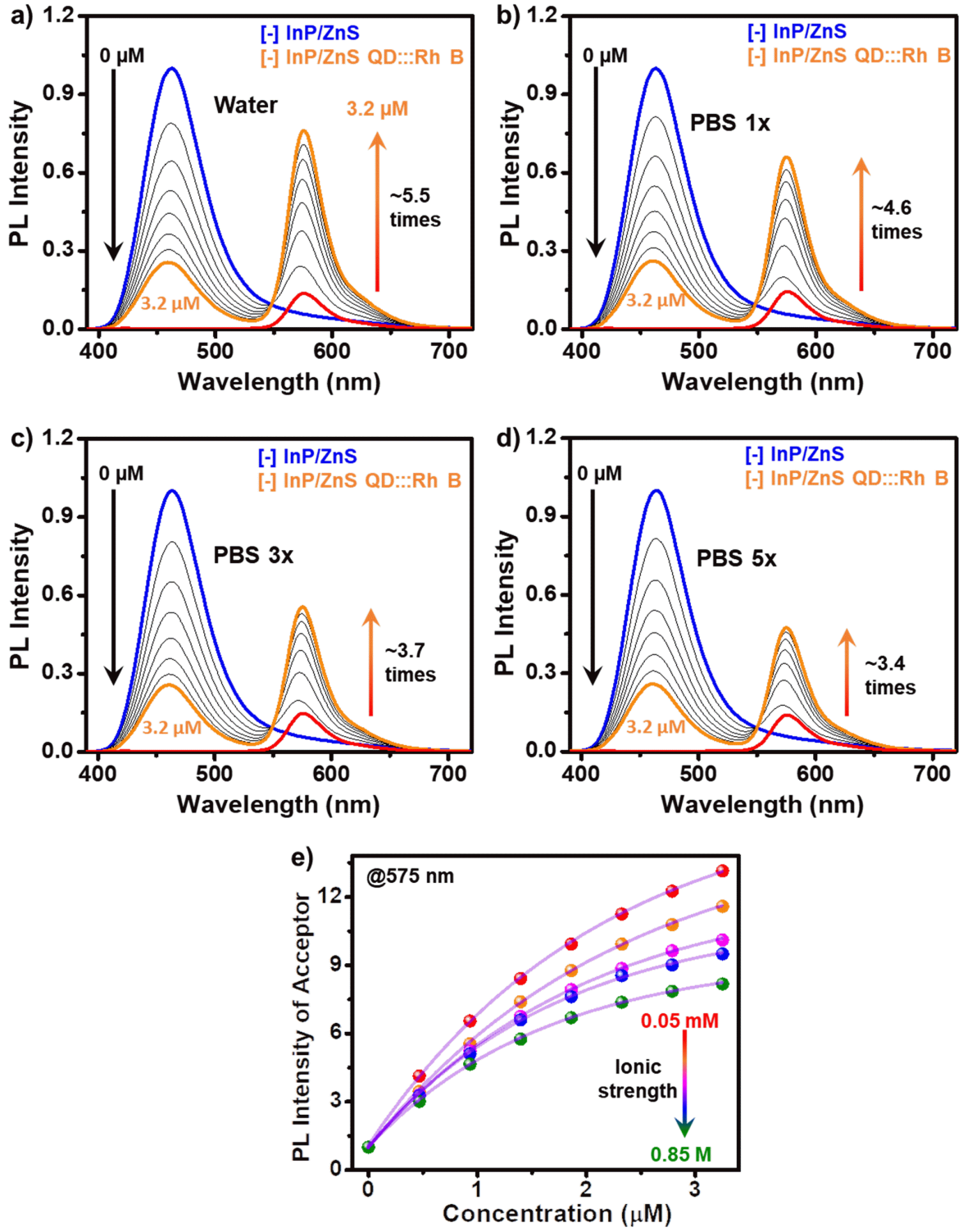

Fig. S26 Proof of **e**lectrostatically driven FRET. PL spectral changes in [-] InP/ZnS QDs upon successive addition of Rh B dye (up to concentration of 3.2 µM) in (a) milli-Q water, (b) 1X PBS, (c) 3X PBS and (d) 5X PBS. (e) The PL enhancement in the acceptor dye decreases with increasing the concertation of PBS solution.

Time-Resolved Analysis

Distance-Dependent Quenching (DDQ) Model: To obtain mechanistic insights into the nature of collisional quenching, a time-resolved Stern-Volmer plot was generated (relative lifetime *vs* acceptor concertation plot). Interestingly, a non-linear behaviour was recorded for time-resolved Stern-Volmer plot as well, which is not a common observation in FRET study. In general, a linear Stern-Volmer is expected from a time-resolved kinetics, where the dynamic component is responsible for the PL quenching process. However, a non-linear Stern-Volmer plot, with a positive curvature, can be attributed to the involvement of more than one quenching mechanism.

To understand further about the mechanism of lifetime quenching process, the model of distance-dependent quenching (DDQ) was taken into consideration, which indicates the involvement of through-space interaction. The DDQ model assumes that the rate of quenching k(r) has an exponential dependence on the distance between donor and acceptor, given by the equation.[31]

$$\boldsymbol{k(r) = k_a e^{\left[-\frac{(r-a)}{r_e}\right]}} \quad \text{... (19)}$$

Where, k_a is the value of k(r) at encounter distance r = a, a is the distance of closest approach, and r_e is the characteristic parameter of the interaction that defines the decrease of k(r) with distance.

Therefore, the rate of collisional quenching will contain a distance component k(r), as shown below.

$$\boldsymbol{\frac{\tau_0}{\tau} = 1 + k(r)\,\tau_0[Q]} \quad \text{... (20)}$$

By substituting the equation (19) in (20), we get

$$\boldsymbol{\left(\frac{\tau_0}{\tau} - 1\right)\frac{1}{[Q]} = k_a\,\tau_0 e^{\left[-\frac{(r-a)}{r_e}\right]} = k'_a e^{\left[-\frac{(r-a)}{r_e}\right]}} \quad \text{... (21)}$$

Now, the plot of "$(\tau_0/\tau\text{-}1)/[Q]$ *vs* r" will be exponential, and will provide the bimolecular quenching (k_a) constant value and the closet distance (a) of quenching for the system (Fig. S27a). Accordingly, the bimolecular quenching constant was estimated to be ~1.24 x 10^{12} $M^{-1}s^{-1}$ using the DDQ model. A higher value of bimolecular quenching constant in comparison with diffusion control quenching rate (typically in order of 10^{10} $M^{-1}s^{-1}$) indicates the presence of strong ground state complexation between donor [-] InP/ZnS QD and acceptor Rh B dye.

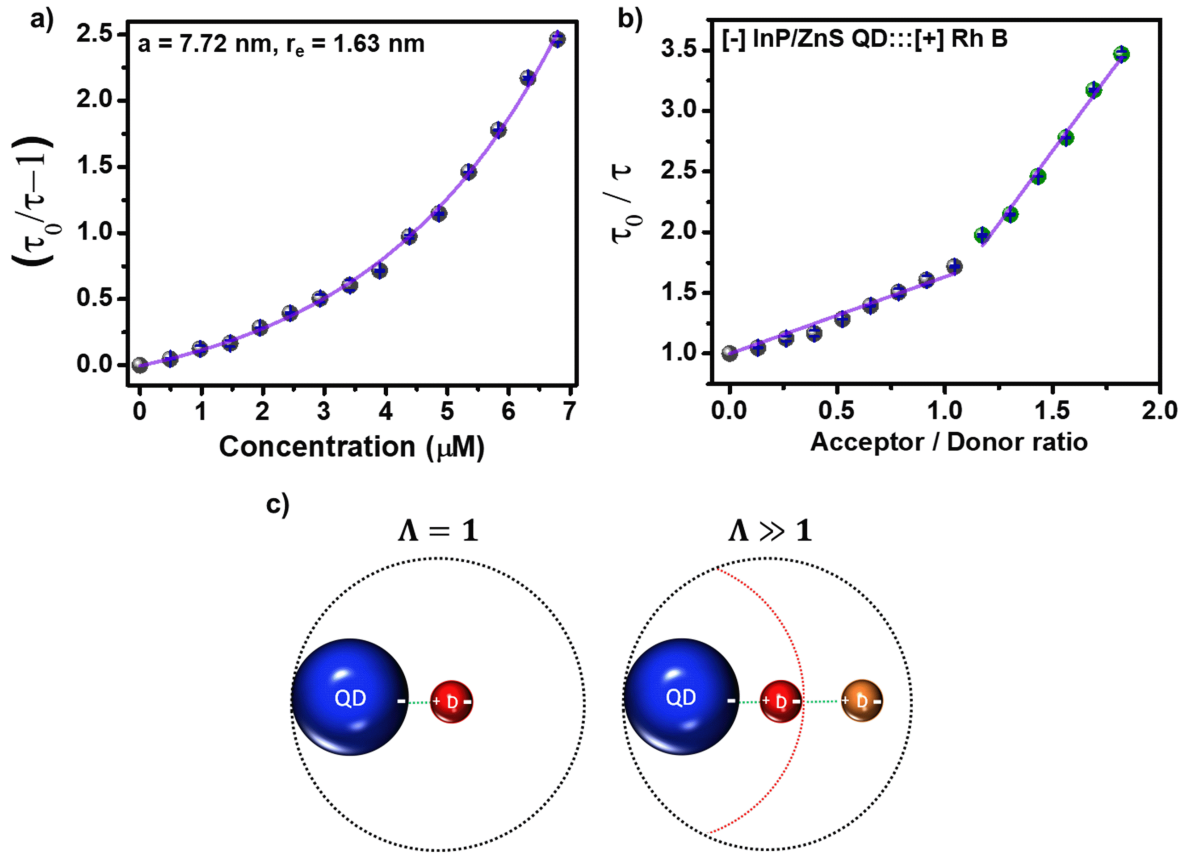

Fig. S27 The DDQ model analysis. (a) the exponential (τ_0/τ-1) *vs* concentration plot proved the best fitting of DDQ model to with a = 7.72 nm and r_e = 1.63 nm, for [-] InP/ZnS QD:::Rh B donor-acceptor system. Perrin's analysis of quenching sphere through the combination DDQ model and Poisson distribution at various number acceptor. (b) the relative lifetime decay of donor [-] InP/ZnS QD as a function of average number of acceptor dye per donor QD. (c) Schematic illustration of interaction between [-] InP/ZnS QD and Rh B dye when Λ = 1 and Λ>>1.

Furthermore, the best fit of lifetime quenching process with DDQ model suggest the presence of more than one acceptor inside the quenching volume, surrounding the donor InP/ZnS QD at diffident distances.

To visualize the probability distribution of Rh B dye surrounding the QD, the Poisson distribution probability was calculated using the following equation.[29]

$$\boldsymbol{P(X = n) = \frac{\Lambda^{n} e^{-\Lambda}}{n!}} \qquad \text{... (22)}$$

Where, Λ represent the concentration ratio of dye to QD, and n is the number of acceptors in closest to QD.

The estimation of Poisson function at different Λ, and fitting of τ_0/τ *vs* Λ plots provides the distribution of acceptor dyes around QDs. The probability of finding average number of acceptors in closet approach to QD is n = 1, at Λ= 1 and remain n=1 even at Λ >> 1. This again

confirms the distance-dependent nature of collisional quenching, and existence of more than one layer of Rh B dye around [-] QD. The presence of dual charges on Rh B dye might helped in formation of multi-layer arrangement through electrostatic interaction. Accordingly, the acceptor distribution was drawn using the value of n and different ratio of dye to QD (Fig. S27c). A negligible change in the zeta potential value was observed for [-] InP/ZnS QD:::Rh B dye complex upon increasing the concentration of Rh B dye, which further proves a multi-layer arrangement of the acceptor molecules.

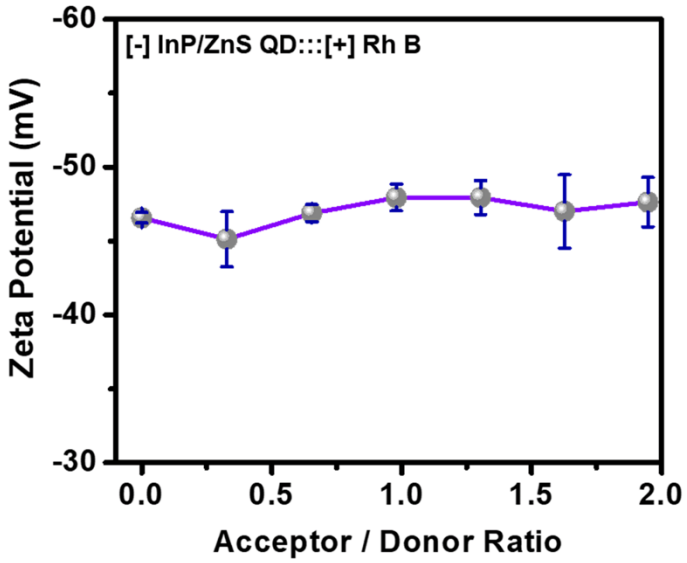

Fig. S28 Zeta potential of **[-]** InP/ZnS QD:::Rh B dye complex as a function of increasing concentration of Rh B dye.

Table S6: PL decay analysis of pure-blue emitting [-] InP/ZnS QDs and [-] InP/ZnS QD:::Rh B dye complex, in a time window of 3.2 µs.

System	τ_1 (ns)	α_1	τ_2 (ns)	α_2	τ_3 (ns)	α_3	τ_4 (ns)	α_4	$\tau_{avg.}$ (ns)	χ^2
[-] InP/ZnS	8.98	0.46	58.42	0.37	167.09	0.15	629.70	0.02	211.63	1.12
[-] InP/ZnS:::Rh B	2.13	0.74	10.40	0.21	47.55	0.04	184.32	0.01	60.80	1.24

Temperature Dependent Lifetime Analysis

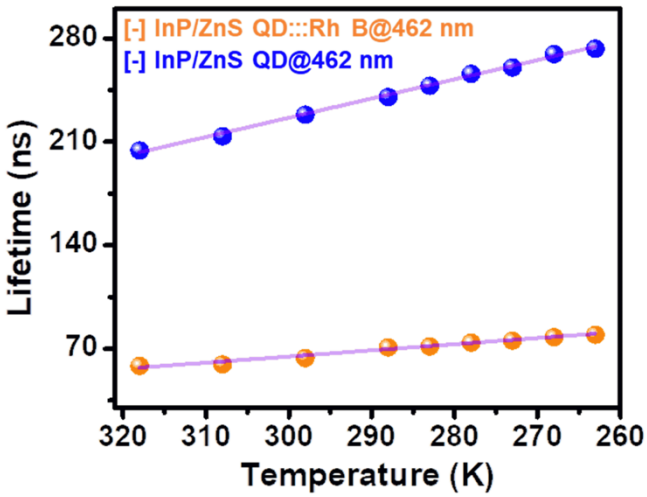

Fig. S29 Temperature dependent lifetime analysis. Variation in the PL lifetime of [-] InP/ZnS QDs in presence (orange) and absence (blue) of Rh B dye in water, as a function of temperature.

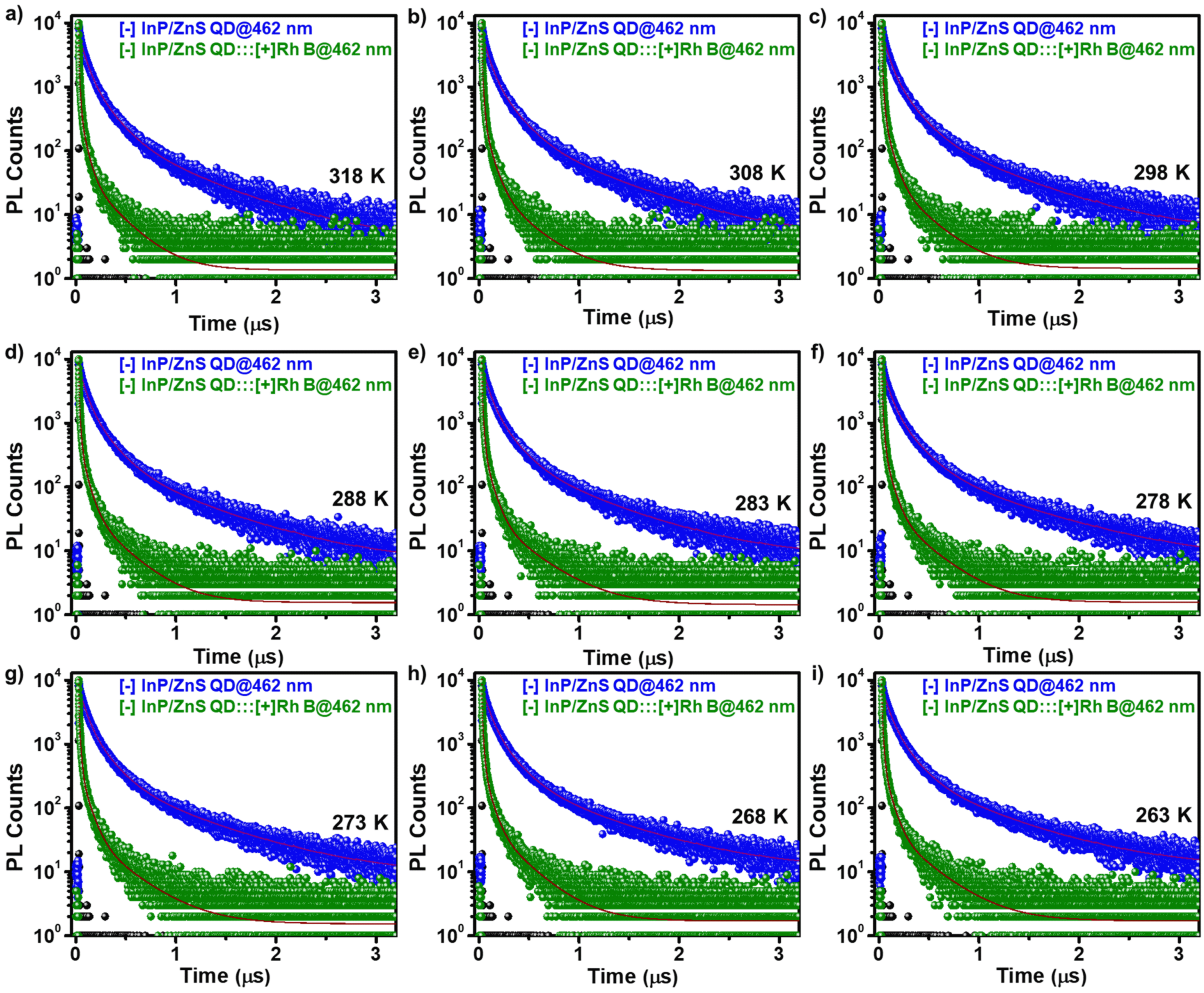

Fig. S30 Temperature dependent lifetime analysis. PL decay profiles of [-] InP/ZnS QD (blue) and [-] InP/ZnS QD:::Rh B dye complex (olive) at different temperatures in water**:** (a) 318 K, (b) 308 K, (c) 298 K, (d) 288 K, (e) 283 K, (f) 278 K, (g) 273 K (h) 268 K and (i) 263 K.

Table S7: PL decay analysis of [-] InP/ZnS QD (blue) and [-] InP/ZnS QD:::Rh B dye complex (orange) at different temperatures, in a time window of 3.2 µs.

Temperature (K)	System	τ_1 (ns)	α_1	τ_2 (ns)	α_2	τ_3 (ns)	α_3	τ_4 (ns)	α_4	$\tau_{avg.}$ (ns)	χ^2
318 K	[-] InP/ZnS	9.48	0.35	58.22	0.45	167.89	0.18	639.45	0.02	204.17	1.12
	[-] InP/ZnS:::[+] Rh B	1.95	0.71	8.42	0.24	37.18	0.04	177.04	0.01	58.27	1.27
308 K	[-] InP/ZnS	11.36	0.37	61.45	0.45	176.02	0.16	670.52	0.02	213.76	1.13
	[-] InP/ZnS:::[+] Rh B	2.23	0.72	9.92	0.23	42.61	0.04	185.32	0.01	59.40	1.31
298 K	[-] InP/ZnS	7.88	0.28	55.68	0.47	160.21	0.22	623.82	0.03	228.28	1.06
	[-] InP/ZnS:::[+] Rh B	2.21	0.69	9.42	0.26	42.69	0.04	196.88	0.01	63.66	1.28
288 K	[-] InP/ZnS	8.04	0.26	58.08	0.49	167.84	0.22	661.19	0.03	240.32	1.08
	[-] InP/ZnS:::[+] Rh B	2.22	0.69	10.07	0.26	46.87	0.04	214.82	0.01	70.84	1.20
283 K	[-] InP/ZnS	9.69	0.28	62.70	0.49	176.65	0.2	681.10	0.03	247.88	1.09
	[-] InP/ZnS:::[+] Rh B	2.00	0.69	9.67	0.26	44.76	0.04	212.32	0.01	71.41	1.34
278 K	[-] InP/ZnS	9.38	0.25	62.21	0.51	178.01	0.21	709.19	0.03	255.99	1.02
	[-] InP/ZnS:::[+] Rh B	2.49	0.69	11.09	0.26	48.84	0.04	228.95	0.01	74.14	1.38
273 K	[-] InP/ZnS	10.62	0.25	65.59	0.52	186.39	0.2	724.50	0.03	260.62	1.07
	[-] InP/ZnS:::[+] Rh B	2.51	0.71	11.91	0.24	53.17	0.04	230.92	0.01	75.44	1.21
268 K	[-] InP/ZnS	10.51	0.25	65.22	0.51	184.92	0.21	748.11	0.03	269.32	1.06
	[-] InP/ZnS:::[+] Rh B	2.45	0.69	11.25	0.26	50.83	0.04	236.93	0.01	77.80	1.32
263 K	[-] InP/ZnS	6.66	0.23	56.69	0.46	158.89	0.27	677.05	0.04	272.98	1.08
	[-] InP/ZnS:::[+] Rh B	2.28	0.67	10.56	0.27	49.60	0.05	240.62	0.01	79.38	1.25

Section 6: Solid-State FRET Studies

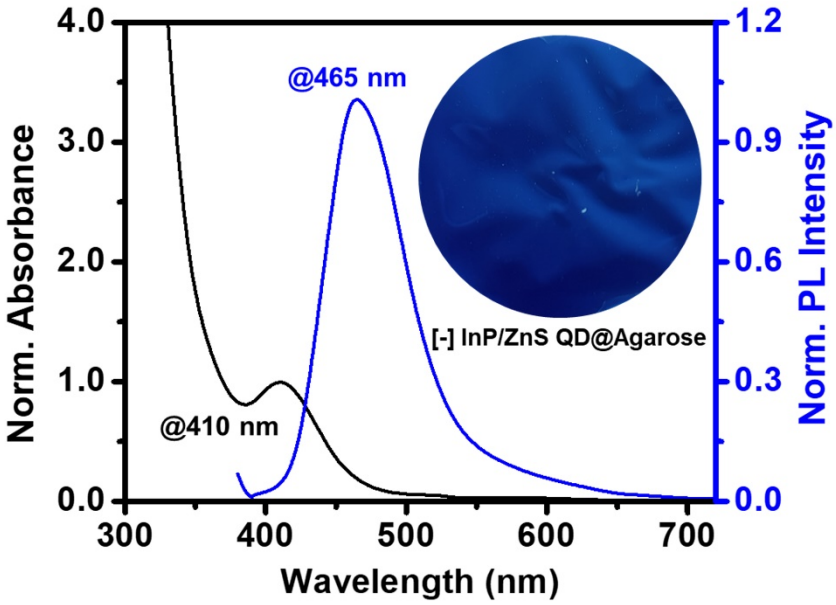

Fig. S31 Characterization of [-] InP/ZnS QDs in agarose film. Normalized absorption and PL spectra of [-] InP/ZnS QDs in agarose film (1%, w/v).

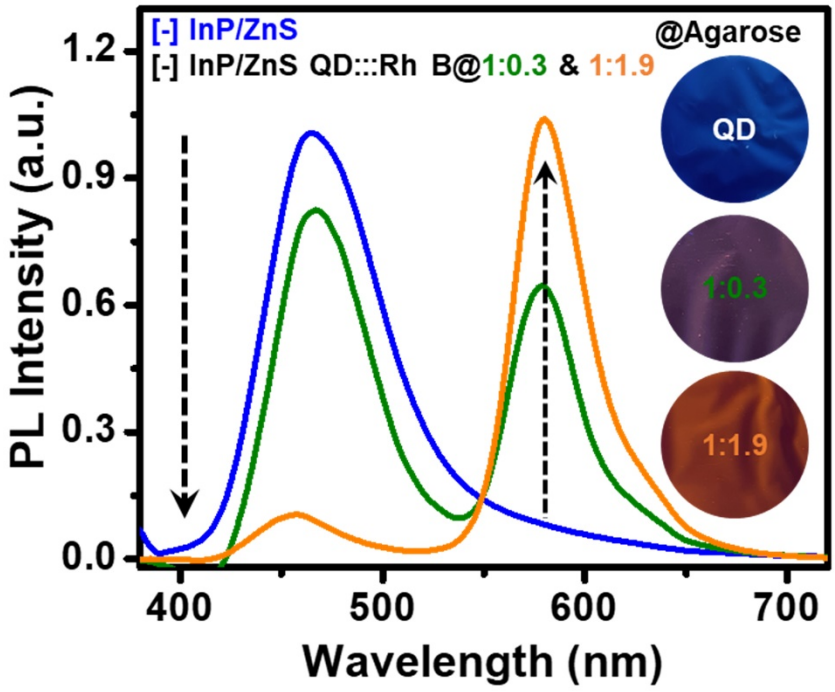

Fig. S32 The solid-state PL spectra of [-] InP/ZnS QDs in absence (blue) and presence (olive & orange) of Rh B dye, in agarose film. The inset shows the true colour PL photograph of corresponding agarose films.

Table S8: PL decay analysis of pure-blue emitting InP/ZnS QDs and [-] InP/ZnS QD:::Rh B dye complex in agarose film, in a time window of 500 ns.

System	τ_1 (ns)	α_1	τ_2 (ns)	α_2	τ_3 (ns)	α_3	τ_4 (ns)	α_4	$\tau_{avg.}$ (ns)	χ^2
[-] InP/ZnS	0.70	0.07	8.39	0.08	52.77	0.43	253.27	0.42	216.85	1.15
[-] InP/ZnS:::Rh B	0.21	0.97	2.50	0.02	12.80	0.01	---	---	4.81	1.40

References

1. W. Zhang, S. Ding, W. Zhuang, D. Wu, P. Liu, X. Qu, H. Liu, H. Z. Wu, K. Wang and X. W. Sun, *Adv. Funct. Mater.*, 2020, **30**, 2005303.
2. G. Devatha, S. Roy, A. Rao, A. Mallick, S. Basu and P. P. Pillai, *Chem. Sci.*, 2017, **8**, 3879–3884.
3. X. Michalet, F. F. Pinaud, L. A. Bentolila, J. M. Tsay, S. Doose, J. J. Li, G. Sundaresan, A. M. Wu, S. S. Gambhir and S. Weiss, *Science*, 2005, **307**, 538–544.
4. A. K. R. Choudhury, In *Principles of Colour and Appearance Measurement*, ed. K. P. Prayagi, Woodhead Publishing, UK, 1st Edn, 2014, Vol. 1, Ch. 7, pp 270–317. DOI: 10.1533/9780857099242.270.
5. X. Lu, H.-Y. Tuan, J. Chen, Z.-Y. Li, B. A. Korgel and Y. Xia, *J. Am. Chem. Soc.*, 2007, **129**, 1733–1742.

6. P. Roy, G. Devatha, S. Roy, A. Rao and P. P. Pillai, J. Phys. Chem. Lett., 2020, 11, 5354–5360.
7. Z. Hens and J. C. Martins, *Chem. Mater.*, 2013, **25**, 1211–1221.
8. I. Moreels, K. Lambert, D. D. Muynck, F. Vanhaecke, D. Poelman, J. C. Martins, G. Allan and Z. Hens, *Chem. Mater.*, 2007, **19**, 6101–6106.
9. J. D. Roo, N. Yazdani, E. Drijvers, A. Lauria, J. Maes, J. S. Owen, I. V. Driessche, M. Niederberger, V. Wood, J. C. Martins, I. Infante and Z. Hens, *Chem. Mater.*, 2018, **30**, 5485–5492.
10. T. Watanabe, Y. Iso, T. Isobe and H. Sasaki, *RSC Adv.*, 2018, **8**, 25526– 25533.
11. H. Mirzai, M. N. Nordin, R. J. Curry, J.-S. Bouillard, A. V. Zayats and M. Green, *J. Mater. Chem. C,* 2014, **2**, 2107–2111.
12. A. L. Patterson, *Phys. Rev.*, 1939, **56**, 978–981.
13. G. O. Eren, S. Sadeghi, H. B. Jalali, M. Ritter, M. Han, I. Baylam, R. Melikov, A. Onal, F. Oz, M. Sahin, C. W. Ow-Yang, A. Sennaroglu, R. T. Lechner and S. Nizamoglu, *ACS Appl. Mater. Interfaces*, 2021, **13**, 32022–32030.
14. A. P. Savintsev, Y. O. Gavasheli, Z. K. Kalazhokov and K. K. Kalazhokov, *J. Phys.:Conf. Ser.*, 2016, **774**, 012118.
15. L. Xi, D.-Y. Cho, A. Besmehn, M. Duchamp, D. Grützmacher, Y. M. Lam and B. E. Kardynał, *Inorg. Chem.*, 2016, **55**, 8381–8386.
16. H. Virieux, M. L. Troedec, A. Cros-Gagneux, W.-S. Ojo, F. Delpech, C. Nayral, H. Martinez, and B. Chaudret, *J. Am. Chem. Soc.*, 2012, **134**, 19701–19708.
17. M. D. Walle and Y.-N. Liu, *Mater. Renew. Sustain. Energy*, 2021, **10**, 1.
18. H.-J. Kang, G. A. K. M. R. Bari, T.-G. Lee, T. T. Khan, J.-W. Park, H. J. Hwang, S. Y. Cho, and Y.-S. Jun, *Nanomaterials*, 2020, **10**, 2012.
19. J. Liu, W. Yang, Y. Li, L. Fana and Y. Li, *Phys. Chem. Chem. Phys.*, 2014, **16**, 4778–4788.
20. K. A. Jackson and W. Schroter, *Handbook of Semiconductor Technology: Processing of Semiconductor*, WILEY-VCH Verlag GmbH & Co. KGaA, Germany, 2000.
21. I. Moreels, K. Lambert, D. D. Muynck, F. Vanhaecke, D. Poelman, J. C. Martins, G. Allan and Z. Hens, *Chem. Mater.*, 2007, **19**, 6101–6106.
22. K. S. Bagdasarov, *Crystallogr. Rep.*, 2002, **47**, S27–S34.
23. S. Rakshit, B. Cohen, M. Gutiérrez, A. O. El-Ballouli and A. Douhal, *ACS Appl. Mater. Interfaces,* 2023, **15**, 3099–3111.
24. Y. Jia, J. Chen, K. Wu, A. Kaledin, D. G. Musaev, Z. Xie and T. Lian, *Chem. Sci.*, 2016, **7**, 4125–4133.
25. J. R. Lakowicz, Principles of Fluorescence Spectroscopy, Springer, New York, 3rd edn, 1999.
26. K. E. Sapsford, L. Berti and I. L. Medintz, *Angew. Chem. Int. Ed.,* 2006, **45**, 4562–4588.
27. P. G. Wo and L. Brand, *Anal Biochem.*, 1994, **218**, 1–13.
28. A. Thomas, K. Sandeep, S. M. Somasundaran and K. G. Thomas, *ACS Energy Lett.*, 2018, **3**, 2368–2375.

29. A. M. Funston, J. J. Jasieniak and P. Mulvaney, *Adv. Mater.*, 2008, **20**, 4274–4280.
30. M. Laferrière, R. E. Galian, V. Maurela and J. C. Scaiano, *Chem. Commun.*, 2006, 257–259.
31. B. Zelent, J. Kuśba, I. Gryczynski, M. L. Johnson and J. R. Lakowicz, *J. Phys. Chem.*, 1996, **100**, 18592–18602.